# Meteotsunamis and other anomalous "tidal surge" events in Western Europe in Summer 2022

E. Renzi ✉ ⓘ ; C. Bergin ⓘ ; T. Kokina ⓘ ; D. S. Pelaez-Zapata ⓘ ; D. Giles ⓘ ; F. Dias ⓘ

🔘 Check for updates

CrossMark

View Online

Export Citation

**Articles You May Be Interested In**

*Sea-Level Science: Understanding Tides, Surges, Tsunamis and Mean Sea-Level Changes*

*Physics Today* (April 2015)

An unconventional tsunami: 2022 Tonga event

*Physics of Fluids* (November 2022)

Modeling of Double Shock Initiation of LX-17 Explosive

*AIP Conference Proceedings* (July 2004)

AIP Publishing

# Meteotsunamis and other anomalous "tidal surge" events in Western Europe in Summer 2022

View Online     Export Citation     CrossMark

E. Renzi,[1,a)] (iD) C. Bergin,[2] (iD) T. Kokina,[2] (iD) D. S. Pelaez-Zapata,[2,3] (iD) D. Giles,[4] (iD) and F. Dias[2,3] (iD)

**AFFILIATIONS**

[1]Department of Mathematical Sciences, Loughborough University, Loughborough LE11 3TU, United Kingdom
[2]School of Mathematics and Statistics, University College Dublin, Dublin D04V1W8, Ireland
[3]Centre Borelli, École Normale Supérieure Paris-Saclay, Gif-sur-Yvette 91190, France
[4]Department of Statistical Sciences, University College London, London WC1E 6BT, United Kingdom

**Note:** This paper is part of the special topic, Physics and Modelling of Tsunamis.
[a)]Author to whom correspondence should be addressed: e.renzi@lboro.ac.uk

## ABSTRACT

We investigate occurrences of anomalous tidal activity in coastal waters of north-west Europe during Summer 2022. Sightings of an anomalous "tidal surge" occurred on 18 June 2022 in Wales, followed by similar observations in Ireland, France, and Spain. Several anomalous long-wave events were also reported in south England and Wales in the morning of 19 July 2022. We analyzed surface and high-altitude air pressure fields, and sea level oscillations for both days. Our detailed analysis reveals that the 18 June events were a series of meteotsunamis, propagating over several countries in Western Europe and triggered by localized pressure perturbations, originating within a low-pressure area over the North Atlantic Ocean. A local analysis of the southern coast of Ireland suggests that Proudman resonance was the determinant mechanism that amplified the meteotsunami traveling eastward in the afternoon of 18 June. A similar analysis of the 19 July events suggests that the tidal surge reported in the UK and anomalous signals recorded in Ireland and France were episodes of seiching triggered by infragravity waves, resonated subharmonically by wind waves. Numerical simulations of the 18 June event were performed with Volna-OP2, which solves the non-linear shallow water equations using a finite volume discretization. The influence of the atmospheric wave velocity on the amplification of the sea surface elevation is analyzed.

## I. INTRODUCTION

This paper investigates several occurrences of anomalous tidal activity in coastal waters of UK, Ireland, France, and Spain during Summer 2022. The first sighting of an anomalous tidal surge occurred on 18 June 2022 in Wales, followed by similar observations in Ireland, France, and Spain. Several anomalous long-wave events were also reported in UK in the morning of 19 July 2022, when tidal surges were observed in south England and Wales.

Anomalous tidal activity, often described by eyewitnesses as a tidal surge or "tidal wave," is usually generated by disturbances acting at the boundaries of the ocean. A disturbance acting at the seabed, such as an underwater earthquake or landslide, can generate destructive tsunamis traveling at the long-wave speed $c = \sqrt{gh}$, where $g$ is the acceleration due to gravity, and $h$ is the water depth in the generation area. Typical tsunamis travel at about 800 km/h and can destroy entire coastlines, such as in the 2004 Pacific Ocean and 2011 Japan events (Levin and Nosov, 2016).

Atmospheric disturbances acting on the ocean surface can also trigger anomalous tidal waves. The most common such waves are meteorological tsunamis (meteotsunamis) and infragravity waves (Bertin et al., 2018).

Meteotsunamis are meteorologically induced long waves in the tsunami frequency range (Monserrat et al., 2006). They are generated by mesoscale atmospheric perturbations traveling offshore, such as squalls, gravitational waves, hurricanes, and weather fronts. As the waves triggered by the perturbation move toward the shore, they are amplified by multi-resonant mechanisms that can drive their amplitude up to several meters. Such mechanisms include the following:

1. Proudman resonance, where a traveling pressure perturbation pumps energy into a wave moving from deeper to shallower water with the same trajectory and speed (Beisiegel and Behrens, 2022; Williams et al., 2021a; Kazeminezhad et al., 2021; Williams et al., 2019).

2. Shelf amplification, where a meteotsunami traveling toward the shore increases in amplitude due to the decrease in water depth.
3. Basin or harbor resonance, where the meteotsunami frequency is close to the resonant frequency of the basin or harbor that it is traveling through (Denamiel et al., 2018).
4. Greenspan resonance, where the speed of a pressure perturbation traveling along the coast is close to the resonant speed of long-shore edge waves.

Once meteotsunamis are amplified by such resonances, they can kill people, destroy harbors, boats, coastal assets, generating damages worth tens of millions of Euro. Catastrophic occurrences include the Vela Luka (Croatia) event in 1978, which resulted in $7 \times 10^6$ Euro worth of damage at that time, the 2006 event in Cuitadella (Spain), which sunk tens of yachts and boats causing damage worth tens of millions of Euro, and the 2017 event in Dayyer (Iran), which inundated about 100 km of coastline, killing five people and injuring 22 (see Monserrat et al., 2006; Šepić et al., 2015; 2016; Thompson et al., 2020; Williams et al., 2021b; Rabinovich et al., 2021, and references therein).

Meteotsunamis are not a rare occurrence in the British isles (O'Brien et al., 2013; 2018; Williams et al., 2019). A historical analysis by Thompson et al. (2020) revealed that there occur on average about ten meteotsunamis per year in the UK, most of them causing little to no damage. A more recent study by Williams et al. (2021b) corrected this estimate to a higher frequency. However, note that the analysis by Williams et al. (2021b) also included winter surges and swells, which have different generation mechanisms than meteotsunamis and were not included by Thompson et al. (2020).

Infragravity waves have lower frequencies than that of common short waves, usually below 0.04 Hz. A typical generation mechanism for infragravity waves is by resonance of incident short wave groups (Ardhuin et al., 2014; Bertin et al., 2018). Because of second-order non-linear interactions, waves in a group traveling at slightly different celerities can force bound long waves that travel phase-locked to the wave group. As the wave system propagates toward shallower water, the long infragravity waves start lagging behind the group of short waves. When the latter break, the infragravity waves are released and travel as free waves (Bertin et al., 2018). Such low-frequency components can then resonate semi-enclosed harbors and basins at their natural frequencies, thus generating coastal seiches.

We remark that the difference between meteotsunamis and infragravity waves is subtle, as they are both atmospherically generated and have similar frequencies. However, note that meteotsunamis are the direct product of atmospheric perturbations (mainly pressure) acting on the ocean surface, whereas infragravity waves are a product of sub-harmonic resonance arising in short wind waves. Moreover, meteotsunamis are the product of multiple resonant phenomena (Monserrat et al., 2006) and tend to be more harmful than infragravity waves.

We also note that storm surges can be affected by additional meteotsunami waves (Shi et al., 2020).

In this paper, we provide an in-depth analysis of met-ocean data referring to 18 June and 19 July 2022. We consider surface and high-altitude air pressure fields, as well as sea level oscillations in an area enclosed by south-west Ireland, Wales, southern England, north-west France, and north Spain. Our analysis shows that the events recorded on 18 June 2022 over several countries in Western Europe were a series of meteotsunamis triggered by pressure fluctuations originating from a low-pressure area north of Ireland. The met-ocean analysis of

19 July gives less defined results. Lack of mesoscale atmospheric perturbations and presence of strong local wind fields across southern UK and Ireland on the same day, suggest that the anomalous tidal surges observed on 19 July could be episodes of seiching in semi-enclosed basins triggered by infragravity waves, resonated subharmonically by wind waves.

This paper is organized as follows: Sec. II presents a description of events that unfolded on 18 June and 19 July 2022, as described by the media, eyewitness reports, and audiovisual material. Section III shows a detailed analysis of surface and high-altitude air pressure fields in Western Europe on both days. In Sec. IV, sea level statistics on data gathered by various tide gauges across Ireland, UK, France, and Spain is presented. In Sec. V, preliminary efforts at numerically simulating the 18 June event over the south of Ireland are presented. The surface pressure disturbance is analytically modeled and a non-linear shallow water solver is used to simulate the generated wave. In Sec. VI, the data presented in the previous sections are further analyzed and discussed, and conclusions are drawn.

## II. DESCRIPTION OF EVENTS

A map with the locations where anomalous tidal surge events were observed on 18 June and 19 July 2022 is presented in Fig. 1(a). In the following, we report the events as they were recounted by eyewitnesses and the media.

### A. Tidal surge events of 18 June 2022

#### 1. South Wales coast

An unusual tidal surge was reported in Solva Harbour (51° 51′ 9.8854″N 5°11′25.232″W) at around 08:50 am on Saturday 18 June 2022.

Local resident Claire Davis said, "At approx 08:50 (an hour before high tide) I looked out of the window and saw that what should have been an incoming tide was in fact ebbing at great speed. The weather was fair and settled. There was a gentle breeze. We watched as this phenomenon continued: water rushing out and then surging back in again. I must stress that the focus of activity appeared to be limited to one area of the harbour here in Solva. Sand was churned up and back eddies were created. Foam developed where the activity was greatest. The surges were thought to be approximately 1 m in height when measured against an iron turning post/mooring post. The cycles of activity lasted ~30 min and then all was calm again and the sand settled. Boats were affected by the forceful flow of water. This caused the boats to list. We estimate the flow of water on inward surges to be 6–8 knots."

Local resident Maggie Studholme reported, "This happened on 18th June between about 9.00 and 9.30 am in Solva. It was not so much a wave as a very fast inrush of water. There is a mooring post on the far side of Solva Harbour and over the course of 2 min, I would estimate that the water level rose maybe 18 in. (45 cm), based on the height of the post. There did not seem to be anything particularly odd about the weather. It was chilly-ish for the time of year, but a lot of this summer has been like that up to that point. It was a bit windy—but again that is very normal for here. Two boats—Jolly Dolly and Talitha—were pushed on their sides by the force of the water. When it was over, we observed the water flowing back out of the harbour faster than usual and declined to go swimming that day."
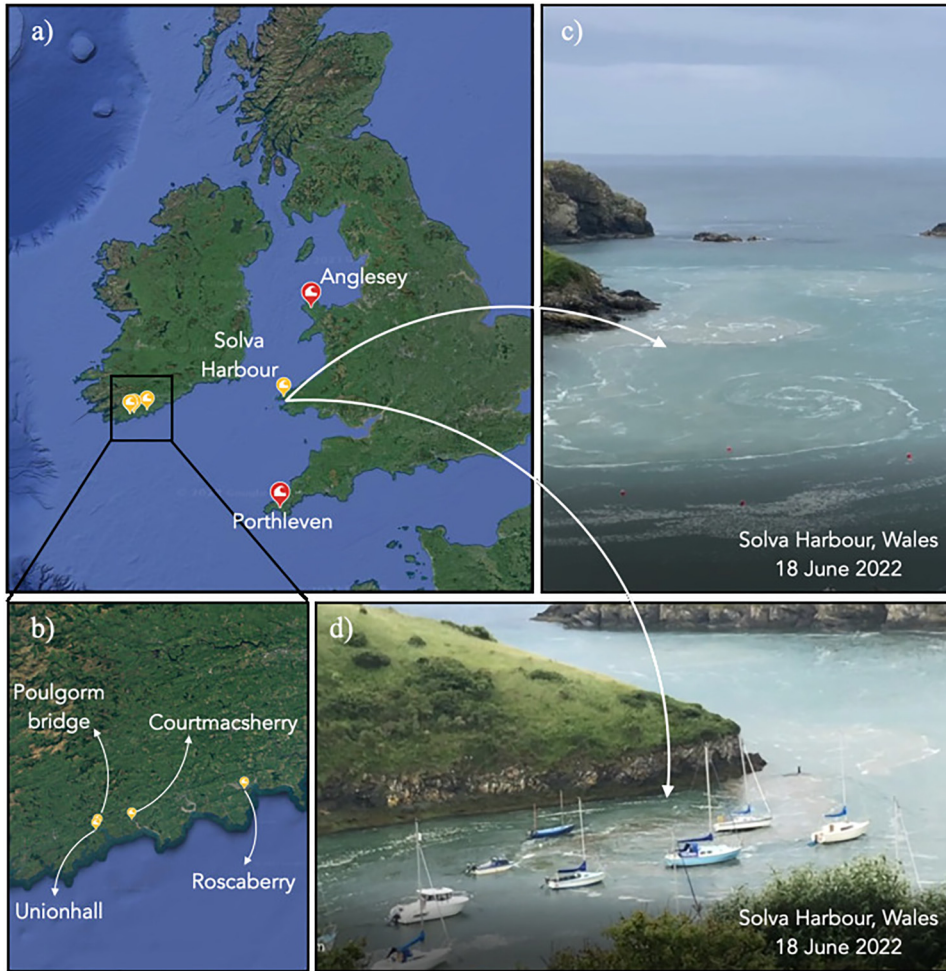
**FIG. 1.** (a) and (b) Map with locations where anomalous tidal surges were observed on 18 June 2022 (yellow markers) and 19 July 2022 (red markers) in UK and Ireland. Note that in Solva Harbour (UK), anomalous events were observed on both days. (c) Still image from footage shot in Solva Harbour (Wales) on 18 June 2022. The generation of a large whirlpool at the entrance of the bay is clearly visible. (d) Same event, water is seen rushing into the harbor and pulling the ships moored there.

Several videos were taken by residents and some stills are depicted in Figs. 1(c) and 1(d). Interestingly, the wave generated a large vortex near the entrance of the bay at Solva Harbour. This is reminiscent (albeit on a much smaller scale) of the large whirlpool generated by the 2011 tsunami in Fukushima (Japan) and described in Dias *et al.* (2014).

### 2. South-east coast of Ireland

Unusual "tidal activity" was sighted in west Cork on Saturday 18 June 2022 (Irish Times, 2022). In the following, we report some key moments as the event unfolded:

- Tide started rushing out of the harbor at Courtmacsherry (51°38'05″N 08°42'33″W) at around 2 pm, when instead it was expected to come in;
- The crew of a boat rowing from Rosscarbery (51°34'40.80″N 09°01'54.12″W) to Union Hall (51°33'29″N 9°08'19″W) reported that at around 3:15 pm, the tide dropped 1.5 m in 5 min and came in and out twice in less than half an hour;
- Eyewitnesses at Poulgorm bridge across the top of the harbor reported, "The tide must have been flowing out at six knots two

hours after low water, and then 6 min later it was coming back in just as fast. It was like tidal bore conditions and changing direction in minutes with mud being carried out to sea."
- In Union Hall, the tide was witnessed going in and out five times over the course of about 3 h and dropping to levels lower than have been witnessed in living memory in Glandore Harbour, locals said.

A first working assumption was that the unusual tide might have been generated by a 2.6 magnitude earthquake recorded at 11:25 am Irish time west of Portugal, about 1900 km southwest of Ireland (Irish Times, 2022). However, the event is not consistent with the low energy of the earthquake and typical tsunami travel time between Portugal and Ireland (NOAA, 2022). Furthermore, there was no reporting of unusual sea levels on the Portuguese coast. Therefore, the only viable hypothesis is that the anomalous tide was generated by atmospheric forcing.

### B. Anomalous long-wave events on 19 July 2022

Another anomalous long-wave event occurred in the same area on 19 July 2022. Local newspapers on the Welsh coast and south coast

of England report on the event using anecdotal evidence, photos, and camera footage, see Daily Post (2022) and Cornwall Live (2022). The event unfolded in the following manner:

- In Cornwall, boats were reported to swing and sway in Porthleven (50°5′7.0944″N, 5°18′57.0708″W) at about 8:45 am. Local residents estimate the water in the harbor to have risen by about a metre in a few seconds, before rushing back out of the harbor. The whole event comprised several oscillations and lasted about 30 min (Cornwall Live, 2022).
- In Wales, an anomalous tide was again seen at Solva Harbour. Local resident Jim Schoenenberger reported, "At around 08:50 am we observed a very sudden and dramatic increase in wind that lasted perhaps 10–15 min. We observed the sea in the bay outside Solva Harbour being whipped up, it looked like force 5–6."
- Swimmers were swept out at sea north of Anglesey (53°16′60.00″N, 4°19′60.00″W). Witnesses on the beach reported rapid water surges, followed by equally rapid retreats (Daily Post, 2022).

To the best of our knowledge, no anomalous wave events were reported on the same day in Ireland and France, and no earthquakes occurred in the area.

Having discounted underwater earthquake sources for the events discussed above, we now consider atmospheric processes with the potential of triggering initial free-surface disturbances, which are then amplified in coastal waters to generate unusual tidal surges.

These dynamics are consistent with several anomalous wave phenomena occurring in the continental shelf zone, of which the most frequent are meteotsunamis and infragravity waves, as already described in Sec. I.

In the following, we analyze mesoscale met-ocean conditions in Western Europe on both 18 June and 19 July 2022 and investigate the nature of the tidal surges described earlier.

## III. ANALYSIS OF SURFACE AND HIGH-ALTITUDE AIR PRESSURE FIELDS

In this section, we present and analyze various data concerning the atmospheric processes that occurred during the events of 18 June 2022 across Ireland, UK, and France. Additionally, after the reports of anomalous surges appearing in England and Wales on 19 July 2022, we analyze the same atmospheric variables in the region on 19 July 2022.

To investigate the nature of these anomalous tidal surges, we follow Rabinovich et al. (2021) and consider atmospheric processes at the surface, 850 hPa and 500 hPa levels, respectively. In particular, we are interested in the presence of fronts: hot, cold, or occluded; wind speed and direction at different levels, and precipitation events and changes in relative humidity. In addition, we investigate the conditions mentioned in Williams et al. (2021b), which are listed as prevailing conditions at the time of most meteorological tsunamis that occurred in Europe between 2010 and 2017. Such prevailing conditions include the following:

- A low pressure area north-west of the UK.
- Most meteotsunamis followed a precipitation event.

- The wave height is greater than or equal to $6\sigma$ of the sea level residual, where $\sigma$ is the standard deviation of the signal [though Monserrat et al. (2006) suggest $4\sigma$].

### A. Events of 18 June 2022

#### 1. Synoptic conditions

Figure 2 (upper panel) shows data for mean sea level pressure (MSLP) and precipitation taken from the 0.5° Global Forecast System (GFS) analysis, issued by the National Oceanic and Atmospheric Administration (NOAA). Note the presence of a low pressure region north of Ireland and the UK, accompanied by a large area of precipitation.

In addition, we accessed ERA5—Fifth generation of ECMWF (European Centre for Medium-Range Weather Forecasts)—atmospheric reanalyzes of the global climate through the Copernicus
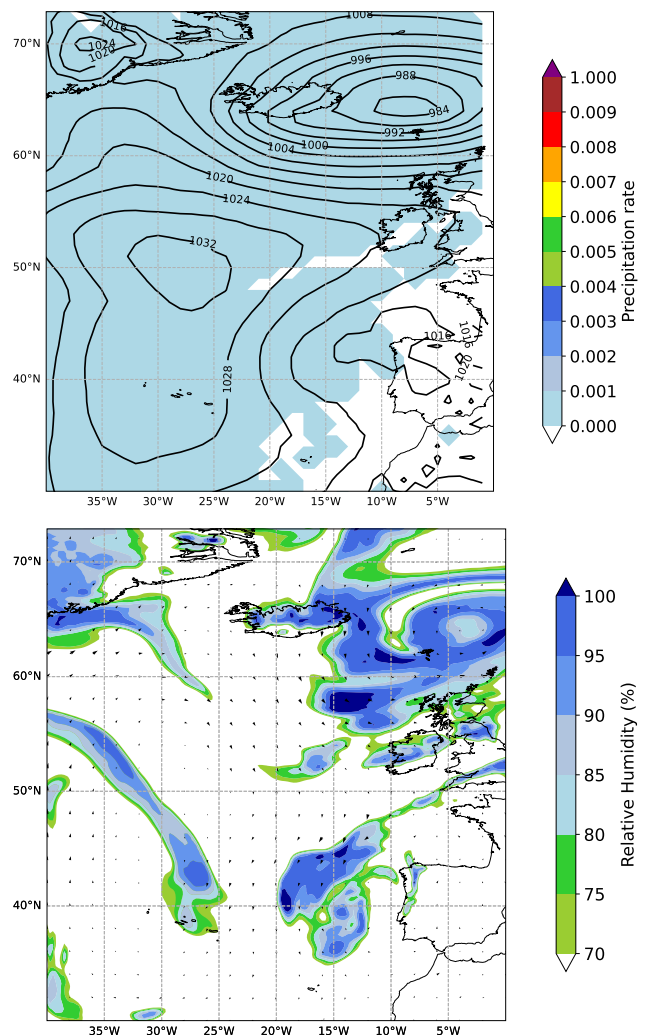


**FIG. 2.** Upper panel: MSLP and precipitation rate from the GFS analysis on 18 June 2022 at midday (12:00). Lower panel: The 850-hPa map of relative humidity.

Climate Change Service Climate Data Store (CDS). Figures 2 and 3 show data for 12:00 UTC on 18 June 2022, in particular, 850-hPa relative humidity (Fig. 2, lower panel), air temperature and wind at 850-hPa (3, upper panel), and high-altitude (500-hPa) wind speed and direction (Fig. 3, lower panel).

The synoptic conditions depicted in Figs. 2 and 3 are reminiscent of similar conditions recorded during historical meteotsunami events. For example, investigating the November 2010, southern Strait of Georgia meteotsunami, Rabinovich et al. (2021) report the presence of sharp pressure gradients in the region, which were the cause of a very intense jet-stream, with wind speeds exceeding 60 m/s. The existence of sharp pressure gradients and a strong jet-stream during the 18 June event, with wind speeds of the same order of magnitude as those reported by Rabinovich et al. (2021), is evident in Fig. 3. Furthermore, Rabinovich et al. (2021) describe the presence of an area of high humidity (>95%) along the south-east border of the jet-stream, which



characterized the 2010 Strait of Georgia meteotsunami. Similarly, the 18 June event features an area of high relative humidity just on the north border of the jet-stream (see again Fig. 2).

We remark that a chain of meteotsunami events recorded over the Mediterranean during 23–27 June 2014 were also accompanied by a pronounced jet-stream shifting eastward (Šepić et al., 2015). A strong jet-stream was also observed during 19–21 March 2017 over the Persian Gulf, whose Iranian side was hit by a violent meteotsunami that killed five people in Dayyer (Heidarzadeh et al., 2020). Interestingly, Kubota et al. (2021), when describing a possible meteotsunami around northeastern Japan, mention the wind condition at heights of ≈500 hPa being ≈40 m/s, which is in very good agreement with Fig. 3. All such similarities suggest that the 18 June 2022 tidal surge events in UK and Ireland were a series of meteotsunamis triggered by the mesoscale atmospheric perturbation described above.

### 2. Near-surface air-pressure disturbances

High resolution, 1-min, air pressure data were collected and analyzed from five weather stations across the south of Ireland (Valentia Observatory, Sherkin Island, Roches Point, Moore Park, and Johnstown Castle). This allowed for the meteotsunami to be identified and tracked across the south coast on 18 June 2022. The air pressures recorded at these stations have not been corrected for mean sea level. This is due to the fact that the altitudes of the weather stations are between 21 and 62 m above sea level. Correcting for these altitudes does not produce significant changes to the results, and the corrections would be removed during the high-pass filtering regardless.

Figure 4 shows the recorded air pressures from the five weather stations across Co. Kerry, Co. Cork, and Co. Wexford. All five records give evidence of a low-pressure system arriving in the late afternoon on 16 June 2022 (not shown in the figure) with lows occurring in the early to mid morning of 17 June 2022, the timing of which being location dependent. The pressure increased over the next 24 h and began to level off. In the afternoon of 18 June 2022, some unusual fluctuations appear at all five locations. This corresponds well with eye witness accounts reporting anomalous tidal activity in that time period (see Sec. II).

The highlighted region of Fig. 4 indicates the 4-h period over which the meteotsunami was observed to affect the Irish coastline. The higher the location is on the graph, the further west the corresponding weather station lies. Inspection of Fig. 4 suggests that the pressure fluctuations traveled from west to east along the coast. This is consistent with the meteorological analysis of McCarthy and Berry (2022).

A high-pass filter was applied to the air pressure data to obtain high-frequency air pressure oscillations, also shown in Fig. 4. In this analysis, a fifth-order Butterworth high-pass filter with a cutoff period of 6 h was chosen. In this case, the filter order ensures that the filter provides a steeper roll-off, that is, it attenuates the frequencies in the stop-band more effectively. The 6-h cutoff period guarantees that the variability associated with larger periods (diurnal or semi-diurnal scales) will be effectively removed or reduced, while those of shorter periods (high-frequency oscillations) will be retained. This means that the filter will remove any low-frequency trends or drifts in the signal (above 6 h), while preserving its high-frequency components such as rapid fluctuations or spikes, which are of great interest for the analysis of the meteotsunami event. The largest fluctuations in the data can be seen at all locations during the time period of interest. The timing of
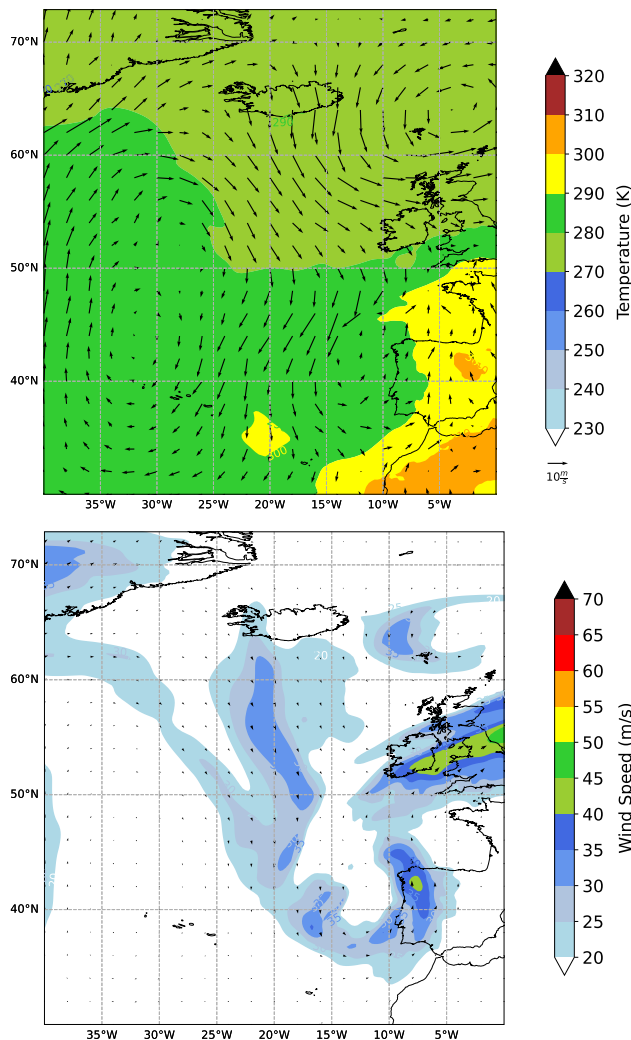
**FIG. 3.** Upper panel: Temperature and wind speed at 850-hPa. Lower panel: High-altitude (500 hPa) map of wind speed and direction; only speeds greater than 20 m/s are colored.
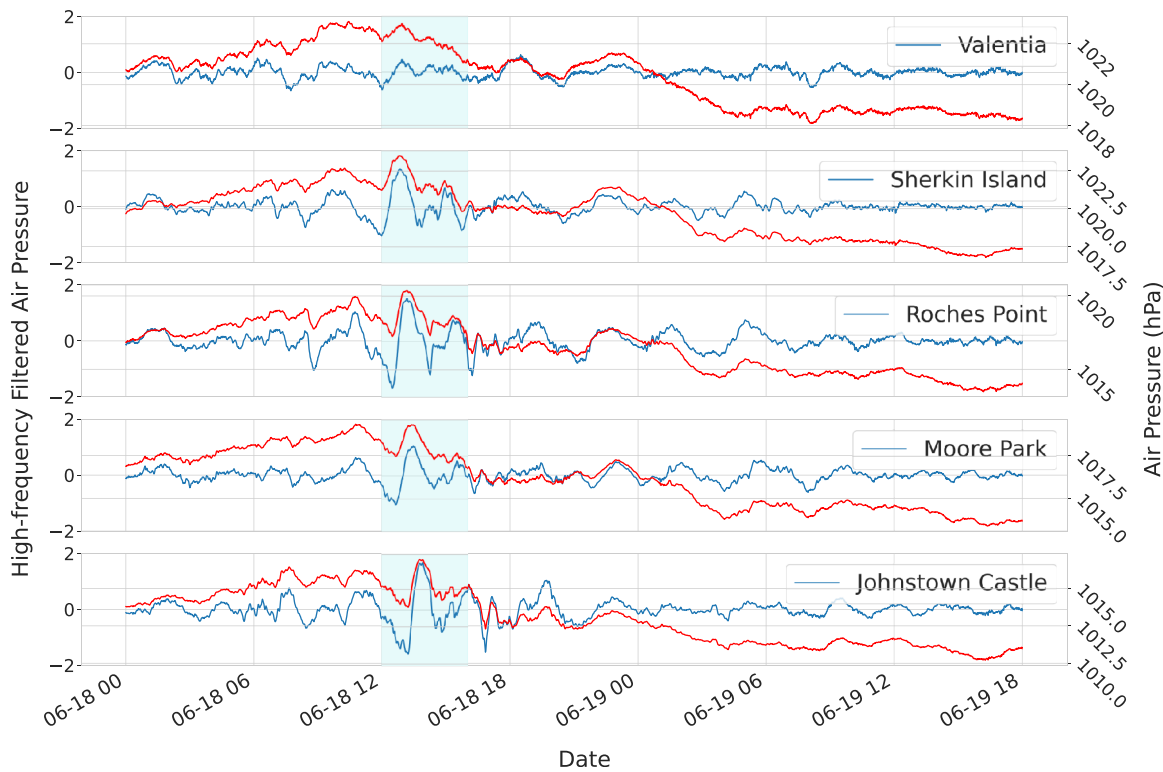
**FIG. 4.** Time series of air pressure above sea level (red line) and high-frequency air pressure data generated by using a 6-h Butterworth high-pass filter (blue line) for all five weather stations across the south of Ireland, between 00:00 on 18 June and 18:00 on 19 June 2022. The highlighted region is the period of time where the meteotsunami was recorded and the corresponding pressure fluctuations can be seen on the graph. Pressure values are in hPa. Online figure in color.

the events varies slightly, but this corresponds well with the locations of the stations from west to east.

We further analyzed the air pressure changes that occurred during a 5-day period, including the event itself. The days analyzed ranged from 16 June to 20 June. The mean pressure change for all stations during this 5-day period was a decrease of the order $\sim 0.4 \times 10^{-3}$ hPa per minute. The median and mode were 0.0 hPa per minute for all five stations, and the atmospheric pressure changes were normally distributed. The largest pressure changes occurred at Roches Point and Johnstown Castle during the afternoon of 18 June. They consisted of an increase of 0.205 hPa per minute and decrease of 0.2 hPa per minute at Roches Point and an increase of 0.184 hPa per minute and a decrease of 0.203 hPa per minute at Johnstown Castle. The maximum variation is approximately 1000 times larger than the mean pressure changes for all five stations.

These data suggest that such strong pressure changes were responsible for the anomalous tidal surge events recorded in Ireland and UK on 18 June 2022. Next, we investigate the frequency components of the atmospheric pressure perturbation.

### 3. Frequency–time analysis

The continuous wavelet transform (CWT) was implemented to analyze the time–frequency characteristics of the atmospheric pressure oscillation associated with the meteotsunami events of 18 June 2022

across the south coast of Ireland. The CWT decomposes a time series into time–frequency space, allowing us to determine both the dominant modes of variability and how those modes vary in time (Torrence and Compo, 1998). The wavelet coefficients are obtained by means of the convolution of the input time signal $x(t)$ and a special function $\psi(t; \tau, \sigma)$, generally known as a mother wavelet,

$$W(\tau, \sigma) = \int x(t) \frac{1}{\sqrt{\sigma}} \psi^* \left( \frac{t - \tau}{\sigma} \right) dt, \qquad (1)$$

where $\sigma$ and $\tau$ represent the frequency scale and time shift parameters, respectively, and the star denotes the complex conjugate. In this particular study, a Morlet function has been chosen as the mother wavelet (see, e.g., Torrence and Compo, 1998). Wavelet power is then calculated as

$$P(\tau, \sigma) = |W(\tau, \sigma)|^2. \qquad (2)$$

Figure 5 shows a clear pulse occurring at approximately midday on 18 June 2022 at several locations on the southern Irish coast, whose location is represented in Fig. 6. According to the time–frequency analysis, the peak power of these atmospheric disturbances lasts in the range of 2–3 h. The pulse appears to occur slightly later in the day as we travel from west to east along southern Ireland, again revealing the trajectory of the associated meteotsunami on the Irish coast. At all stations, the atmospheric perturbation exhibits a primary period of about 2–3 h, with secondary oscillations at longer periods.
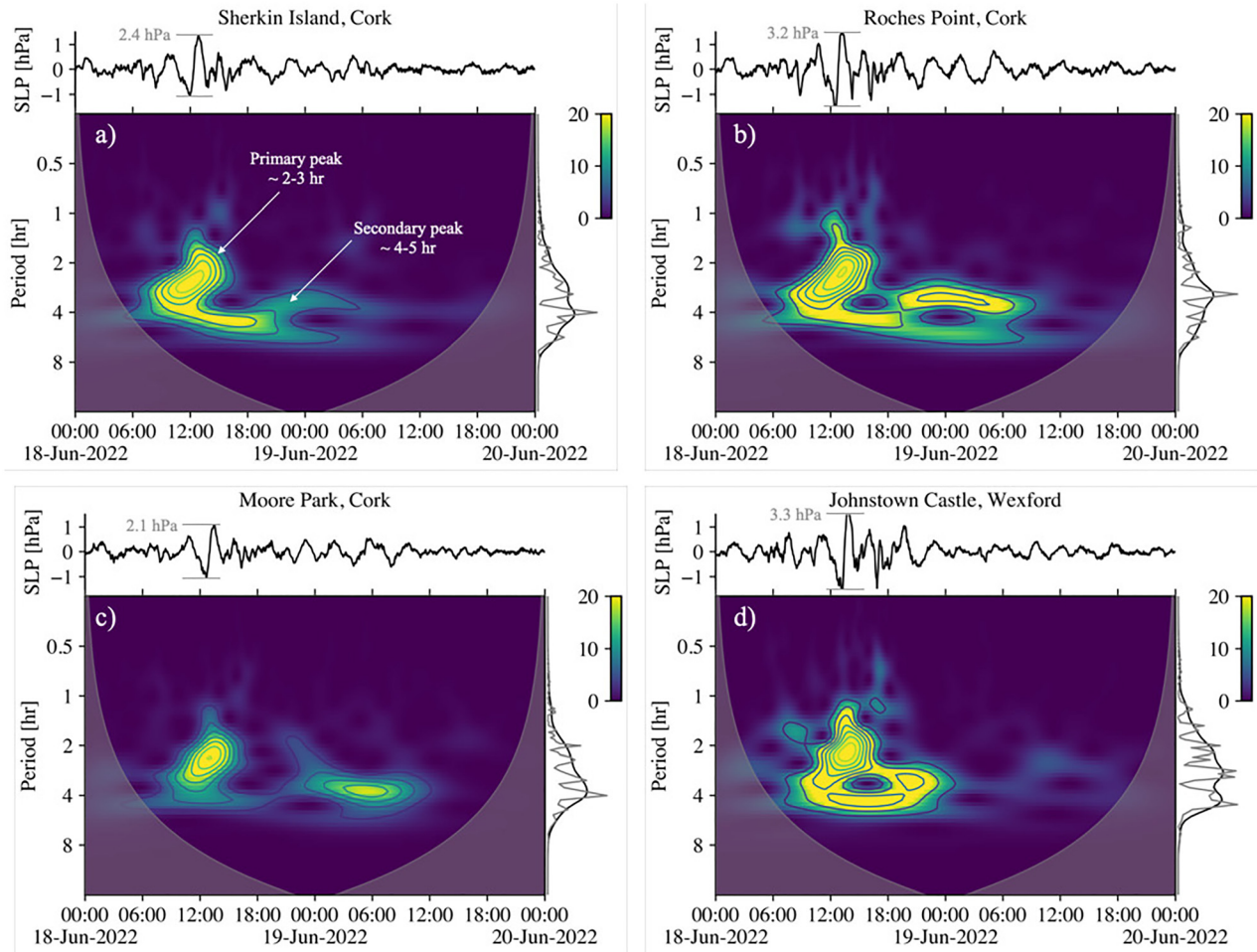
**FIG. 5.** Wavelet power spectrum of the sea surface air pressure signal measured at several stations across the south of Ireland: (a) Sherkin Island, (b) Roches Point, (c) Moore Park, and (d) Johnstown Castle. In each panel, the color scale indicates the wavelet power spectral density in hPa²/cph, where cph means cycles per hour. The shaded gray area corresponds to the cone of influence. The top insert panel shows the time series of the high-pass filtered sea surface atmospheric pressure in hPa. The right insert illustrates the time-integrated wavelet power (black line) and the Fourier power spectrum (gray line). The location of the stations is depicted in Fig. 6.

## 4. Characteristics of the surface pressure disturbance

Lagged cross-correlation analysis was performed over the mean sea level records at different stations of the Irish weather network. This statistical technique is generally used to examine the relationship between two signals or series as a function of time delay. It measures their similarity as a function of the time lag between them. Lagged cross-correlation is used here to identify the time delay between two signals that are related but not perfectly synchronized, by finding the maximum correlation between the two signals when one is shifted in time relative to the other. The resulting cross-correlation function is a measure of how well the two signals match up, with higher values indicating a stronger relationship. This analysis allows us to estimate the propagation of the atmospheric perturbation across the different stations. The Sherkin Island station was taken as a reference, since the perturbation was first observed at this station. Figure 6(a) shows the lagged cross-correlation with respect to Sherkin Island and the

associated time lag. All stations in which the maximum cross-correlation was less than 0.6 were not considered in the analysis [represented by the black points in Fig. 6(b)]. Notice that the atmospheric perturbation was initially observed at Sherkin Island, 25 min later at Roches Point with a correlation of 0.82, then 36 min later at Moore Park with a correlation of 0.80. After approximately 1 h, the same perturbation was observed around the east coast of Ireland (Johnstown Castle and Oak Park), but the correlation dropped to around 0.7. Figure 6(b) shows a map with all stations where the correlation with respect to Sherkin Island was higher than 0.6.

Assuming that the atmospheric disturbance occurred at a synoptic scale and was uniform in the direction perpendicular to the direction of propagation, we can estimate the velocity vector of the wave disturbance, given the time delay and the distance between stations. First, the phase difference of a planar wave passing by two stations $m$ and $n$ can be written as
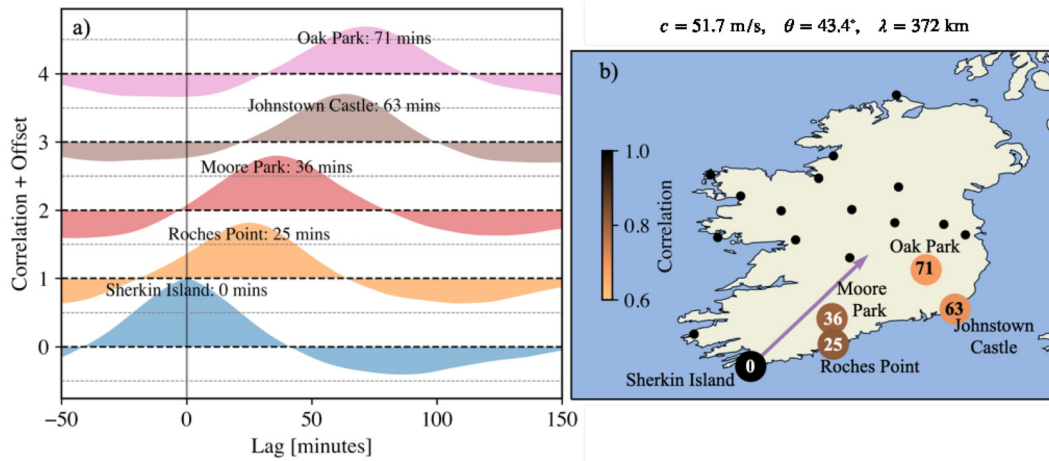
**FIG. 6.** (a) Cross-correlation between surface pressure data recorded by the Irish weather station network. (b) Map of the stations. The color scale represents the maximum correlation with respect to the Sherkin Island station, and the circled numbers indicate the associated time lag in minutes. The arrow indicates the estimated direction of the pressure disturbance traveling along the southern Irish coast, based on the cross-correlation analysis. Only correlations above 0.6 were considered.

$$\Delta\phi_{mn} = \mathbf{k} \cdot \Delta\mathbf{x}_{mn} = kr_{mn}\cos(\theta - \alpha_{mn}),$$

where $k$ and $\theta$ are the wave number magnitude and direction of the wave disturbance, respectively, $r_{mn}$ is the radial distance between two points, and $\alpha_{mn}$ is the orientation angle with respect to the east. Note that only a set of three points are required in order to solve for the two unknown variables (wavenumber $k$ and direction $\theta$). Hence, we obtain

$$\Delta\phi_{mn} = kr_{mn}\cos(\theta - \alpha_{mn})\Delta\phi_{mp} = kr_{mp}\cos(\theta - \alpha_{mp}).$$

The phase $\Delta\phi_{mn}$ and time lag $\Delta t_{mn}$ are linked through the relationship $\Delta\phi_{mn} = 2\pi f \Delta t_{mn}$, where $f$ is the frequency of the atmospheric wave perturbation, which varies from $f = 1/2$ to $1/3$ cycles/hour, according to the time–frequency analysis presented in Fig. 5. The phase speed is $c = 2\pi f / k$.

The results indicate than in the south of Ireland, the pressure perturbation was traveling at a speed of $c = 51.7\,\mathrm{m/s}$ and at an angle of around $\theta = 43.4°$ measured counterclockwise from the east. This atmospheric perturbation had a typical wavelength of $\lambda = 2\pi/k = 372$ km. Considering a depth of the continental shelf of Ireland ranging from 150 to 300 m, we estimate that the long water wave should travel at a speed of $38 - 54\,\mathrm{m/s}$, which is nearly the speed of the atmospheric wave. This suggests that Proudman resonance was the determinant mechanism that amplified the meteotsunami along the southern coast of Ireland. These results are in accordance with those reported previously by Tanaka (2010), who, by means of numerical simulations of an event over the East China Sea with similar characteristics, found that the propagation speed of the atmospheric wave was $25 - 30\,\mathrm{m/s}$.

### B. Anomalous long-wave event on 19 July 2022

Following the same procedure as in Sec. III, we now analyze the regional atmospheric situation on 19 July 2022. The data are taken from CDS and is part of the ERA5 reanalysis for July 2022.

Figure 7 (upper panel) shows the surface weather map over Western Europe on 19 July at 8:00 am. Note that, unlike on the 18

June, there are no areas of low atmospheric pressure in the region. Figure 7 (lower panel) shows the 850-hPa map of relative humidity and wind velocity over Western Europe. A number of regions of high humidity (>95%) are clearly visible in the reanalysis. However, unlike the 18 June, there are no regions of high humidity directly above the UK and Ireland. Finally, Fig. 8 shows the temperature and wind speed at 850-hPa (upper panel), and the wind speed and direction at 500-hPa (lower panel). Note that no high-altitude jet-stream is present in the area at the time the anomalous surge was observed. Therefore, the synoptic conditions in Figs. 7 and 8 do not display any of the characteristic conditions that are usually associated with meteotsunami occurrence in Europe. While this fact does not rule out the possibility that the 19 July event was also a meteotsunami, local measurements would suggest that this event was more localized and of a different nature than the 18 June meteotsunamis.

Figure 9 (upper panel) shows the time series of wind speed, gust, and direction at St. Ann's Weather Station in Wales. This station is installed on the Mid Channel Rock Lighthouse beacon just off St. Ann's Head, at location 51° 40.315 N 5° 9.826 W. It is owned and maintained by Milford Haven Port Authority. Note the rapid increase in wind speed and gusts at around 8:45 am on 19 July. As for the wind rose, its direction veered through 80° in about 30 min. Figure 9 (lower panel) shows the time series of humidity, temperature, and dew point at the same station, between 18 and 19 July 2022. Note the fast decrease in temperature from 6:00 am to 8:00 am on 19 July, accompanied by a fast increase in humidity.

The presence of strong winds in the area, together with the lack of noticeable phenomena at the mesoscale, reveal that the 19 July event was more localized than the 18 June meteotsunamis described above. This event could be a small scale meteotsunami, as the local increase in humidity would suggest, or also a long wave resonated by infragravity waves, triggered by the rapid increase in wind speed (Ardhuin et al., 2014). It is worth noting that infragravity waves are among the most common mechanisms driving coastal seiches in semi-enclosed basins (Bertin et al., 2018). For example, strong seiches regularly occur
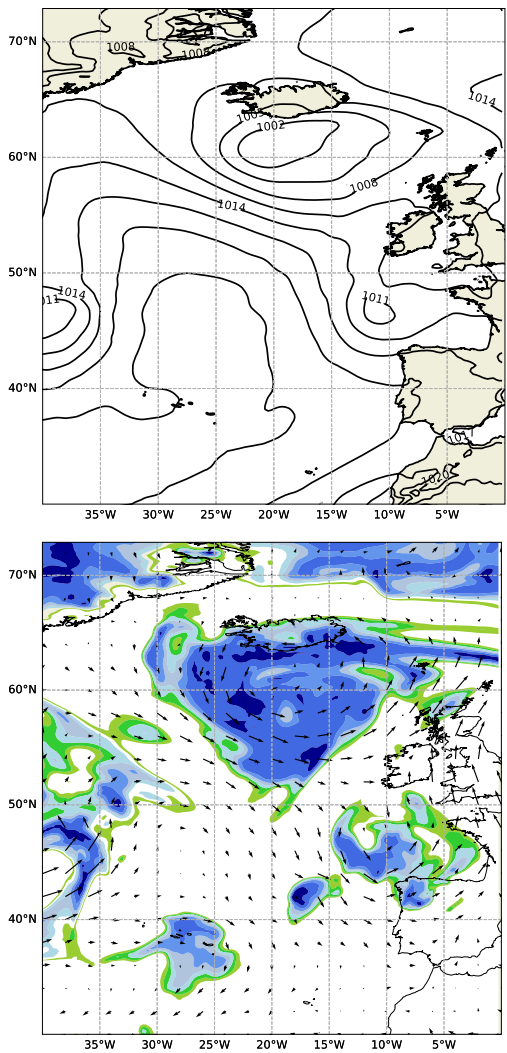
**FIG. 7.** Upper panel: The surface weather map on 19 July 2022 at 8:00 am. Lower panel: The 850-hPa map of relative humidity and wind velocity.



**FIG. 8.** Upper panel: Temperature and wind speed at 850-hPa. Lower panel: High-altitude (500-hPa) map of wind speed and direction; only speeds greater than 20 m/s are colored.

in Port-Tudy harbor, located on Groix Island (west coast of France), as a result of non-linear resonant amplification of infragravity waves. It is possible that the rapid increase in wind speed on 19 July has generated trains of short waves. Those could have interacted subharmonically to generate infragravity waves of periods close to the resonant period of semi-enclosed coastal basins in south England and Wales, where the phenomenon was reported (see again Sec. II). Infragravity wave periods can be as high as 5 min, which is close to the resonant period of typical semi-enclosed natural basins (Bertin *et al.*, 2018). Therefore, the 19 July event is consistent with the development of seiches resulting from the amplification by resonance of infragravity waves.

## IV. ANALYSIS OF SEA LEVEL OSCILLATIONS

### A. Sea level statistics

Sea level oscillations were examined for the meteotsunamis of 18 June 2022 and the event of 19 July 2022. We followed the method of
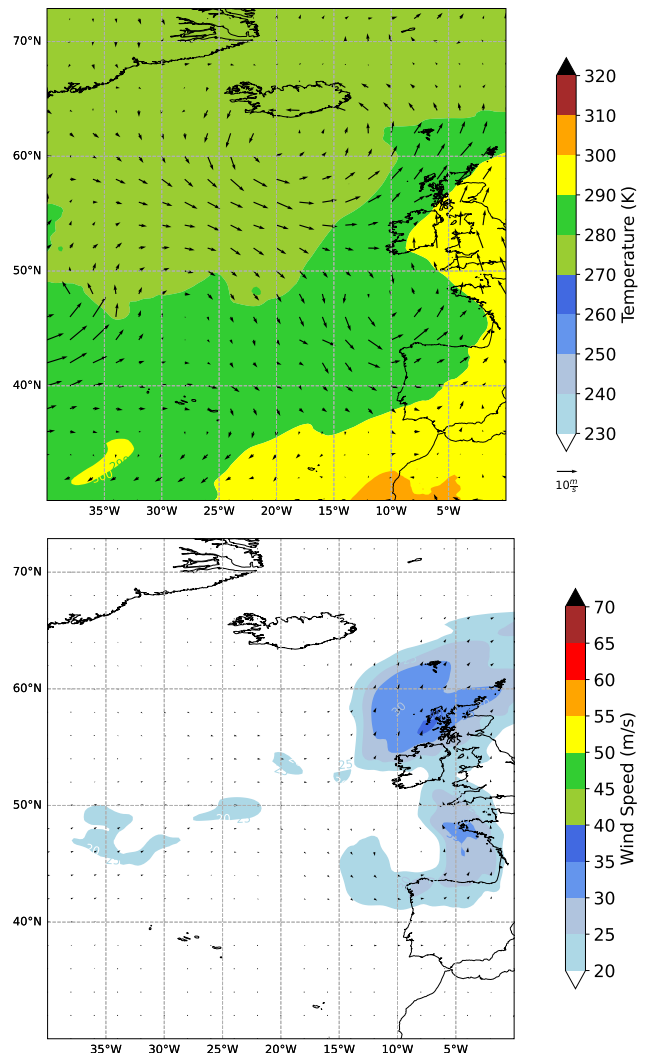
Rabinovich *et al.* (2021) and Thomson and Emery (2014) to obtain de-tided, filtered data for the sea level oscillation.

### 1. Meteotsunamis of 18 June 2022

For better understanding and visualization of the events, Fig. 10 presents the map of locations of all the tide gauges used in the following analysis.

The data presented in Fig. 11 was obtained from tide gauges located on the south and south-east coasts of Ireland, and is available through UNESCO Sea Level Monitoring facility (UNESCO, 2022). Data are recorded every 5 min. Anomalous sea level oscillations associated with the meteotsunami traveling eastward along the south coast of Ireland in the afternoon of 18 June 2022 are clearly visible in those figures.
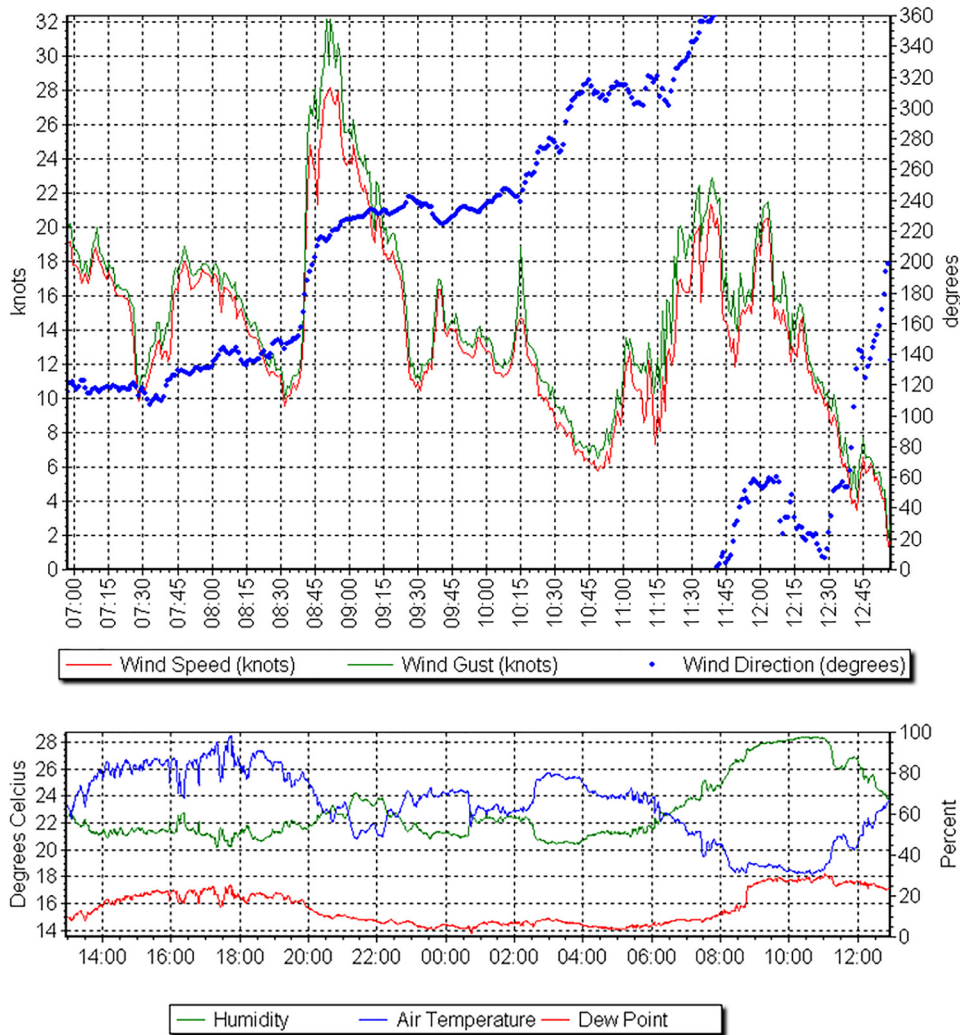
**FIG. 9.** Meteorological data at St. Ann's Weather Station (Wales) on 19 July 2022. Upper panel: Wind speed, gust, and direction. Lower panel: Humidity, air temperature, and dew point. Data extracted from www.stannsweather.org.uk.

Similar to the filtering of the atmospheric data, tide gauge data were filtered using a fifth-order Butterworth high-pass filter with a cut-off period of 3 h, as we wanted to remove naturally occurring tides of periods of above 3 h.

Figure 12 shows the tidal gauge data for Milford Haven (51.7143° N, 5.0427° W) in Wales, provided by the British Oceanographic Data Centre (BODC). No particular anomalies can be seen during the morning of 18 June 2022 (though there are some spurious oscillations occurring in the afternoon of 18 June and through the following day), despite the fact a meteotsunami event was clearly observed in the area at that time (see Sec. II). We remark that tidal gauge data in the UK are recorded at 15-min intervals, not in real-time like other European countries. Most basin oscillations triggered by meteotsunamis have periods of 1 to 10 min; therefore, the technology currently being used in the UK does not allow for the recording of such events. In light of an increasing meteotsunami activity in the North Atlantic Ocean (Thompson *et al.*, 2020; Williams *et al.*, 2021b), it is strongly advised that the UK adopts real-time recording of tidal gauge data.

Looking outside Ireland and the UK, anomalous oscillations in the tide gauge data in France and Spain were recorded as well.

At Les Sables-d'Olonne, Fig. 13 (second panel), there is a clear meteotsunami signature on 18 June at around 6:25 pm. In Ouistreham, Fig. 13 (forth panel), there are a few spikes before the first event, but from around 8:00 pm on 18 June, a constant presence of anomalous oscillations can be noticed. At Le Havre, Fig. 13 (top panel), where only 5-min tide gauge data are available, a strong meteotsunami signature is clearly visible on the evening of 18 June. In Dieppe, Fig. 13 (third panel), prominent changes in relative sea level start appearing around 9:00 pm on 18 June.

In Spain, oscillations appear in the Gijon tidal gauge recordings, as shown in Fig. 14. Such oscillations start from the afternoon of 18 June 2022 and continue throughout the following day.

In summary, tidal gauge data confirm that the 18 June events were a series of meteotsunamis, propagating over several countries in Western Europe (Ireland, UK, France, and Spain) and triggered by localized pressure perturbations originating within a low-pressure area
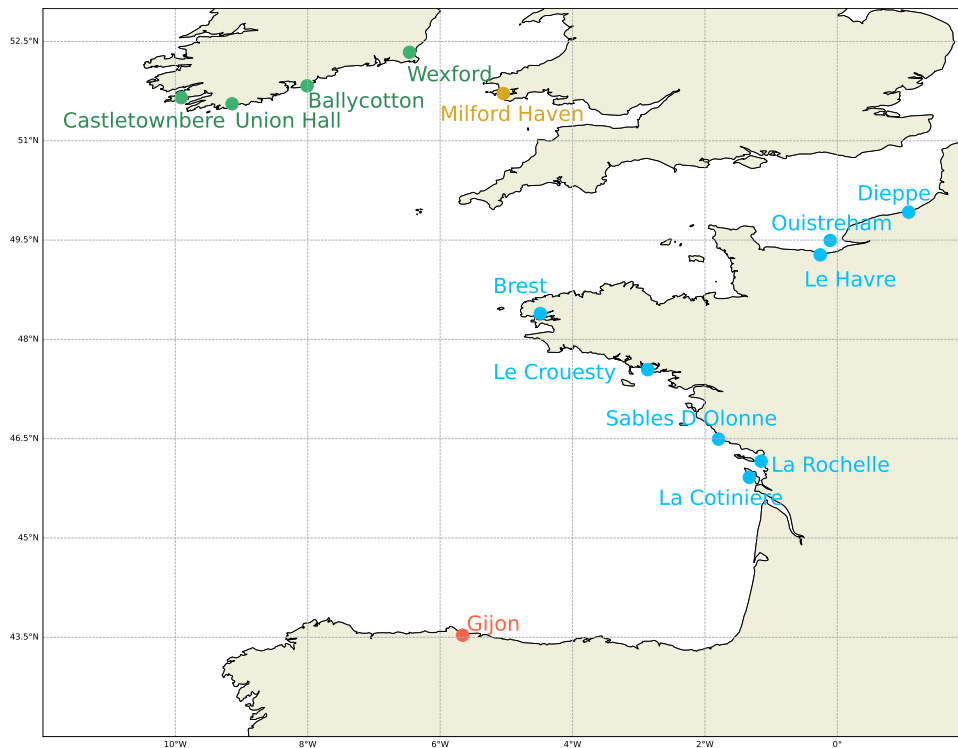
**FIG. 10.** Map of the tide gauges used in the analysis of the 18 June event.

on the North Atlantic Ocean (see Sec. III). Such phenomena were accompanied by thundery outbreaks in parts of southern England and northern France (Sibley, 2022; McCarthy and Berry, 2022).

### 2. Events on 19 July 2022

As mentioned in Sec. III, anomalous tidal surges were reported in south England and Wales in the morning of 19 July 2022. We are not aware of reports of similar events in Ireland or France. We already presented the overall atmospheric situation in Sec. III. In this section, we analyze the tide gauge data using the same method as above.

Figure 15 shows the record from the tidal gauges around the south coast of Ireland in the same locations as those considered earlier for the 18 June event. Anomalous oscillations are visible in Ballycotton (second panel) and Union Hall (third panel from the top). On the other hand, Castletownbere (first panel) has some oscillations around the time of the event, but they are not as prominent as in Ballycotton and Union Hall. Wexford (last panel) has very small disturbances, but they are still visible. Still in Fig. 15, large spikes appear in all de-tided and high-pass filtered records between the evening of 19 July and the early morning of 20 July, highlighted by the solid ellipse. However, all tide gauges are missing data in that time period: there are no records between ∼7:00 pm and ∼11:30 pm on 19 July. Therefore, results in the circled region are not reliable.

Figure 16 shows de-tided and high-pass filtered records at various locations along the north coast of France (see again the map of Fig. 10). In Brest, Fig. 16 top panel, very clear oscillations start at around 5.00 am on 19 July 2022 and last throughout the following

day. At Le Crouesty, Fig. 16 bottom panel, obvious anomalies start at around 7:00 am and last throughout the morning of 19 July. In Les Sables-d'Olonne, Fig. 16 middle panel, there is an obvious disturbance starting at around 10 am on the same day. Data analyzed at La Rochelle, Le Havre, and Gijon are inconclusive and is not shown here.

We remark that relatively strong winds were present in the Bay of Biscay and around the north-Atlantic coast of France in the morning of 19 July 2022, as shown in Fig. 8. Wind is usually not a direct forcing mechanism for meteotsunamis, except in very shallow basins (Šepić *et al.*, 2015). The presence of relatively strong wind and the absence of mesoscale atmospheric perturbations on 19 July (see again Sec. III) suggest that the tidal surge events reported in the UK and the anomalous signals recorded in Ireland and France could be episodes of seiching triggered by infragravity waves, resonated subharmonically by wind waves. However, note that the distinction between meteotsunamis and infragravity waves is very subtle, as they have similar period ranges, are both generated atmospherically, and can manifest in very similar ways.

### B. Time–frequency analysis

The CWT has also been used to investigate the time–frequency characteristics of the sea level data recorded across the south west of Ireland during the 18 June meteotsunami (see Sec. III A 3). Figure 17 shows the wavelet power spectrum corresponding to the observed sea level data at Ballycotton, Wexford, Union Hall, and Castletownbere, respectively. Sea level signals were high-pass filtered using a fifth-order Butterworth filter with a 4-h cutoff period. This filter removes the low-frequency oscillations associated with astronomical tide.
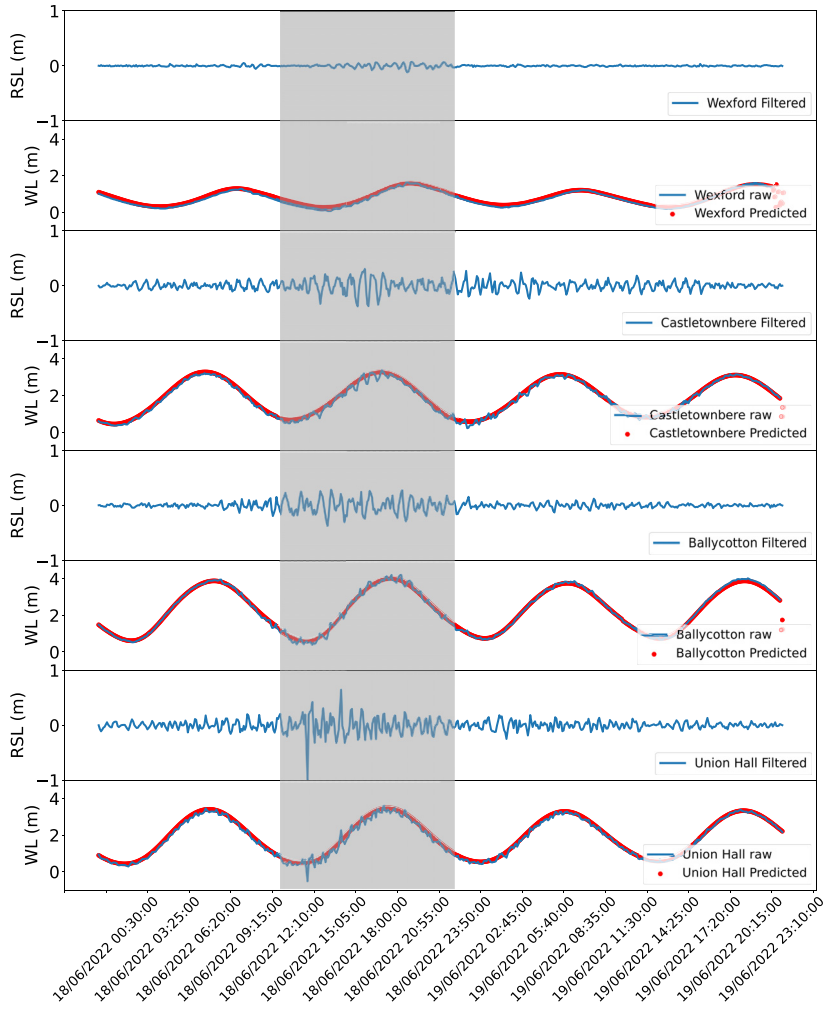
**FIG. 11.** De-tided and high-pass filtered (Butterworth) records of the event of 18 June 2022 at several locations in Ireland. The bottom plot of each panel shows the predicted versus the observed sea water level at the tide gauge. The approximate time of the event is highlighted in gray. WL = water level, RSL = real sea level.
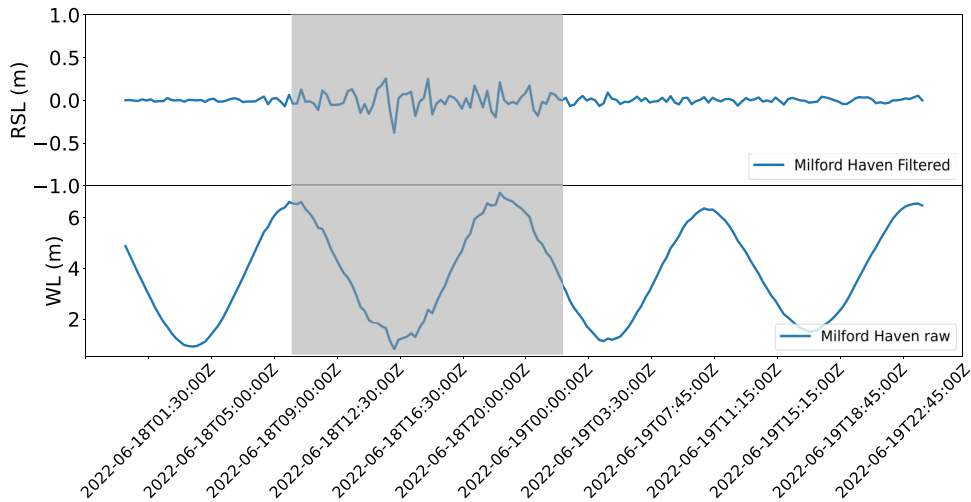


**FIG. 12.** De-tided and high-pass filtered (Butterworth) records of the event of 18 June 2022 at Milford Haven. The bottom plot shows the raw observed sea water level at the tide gauge. Data are recorded every 15 min.
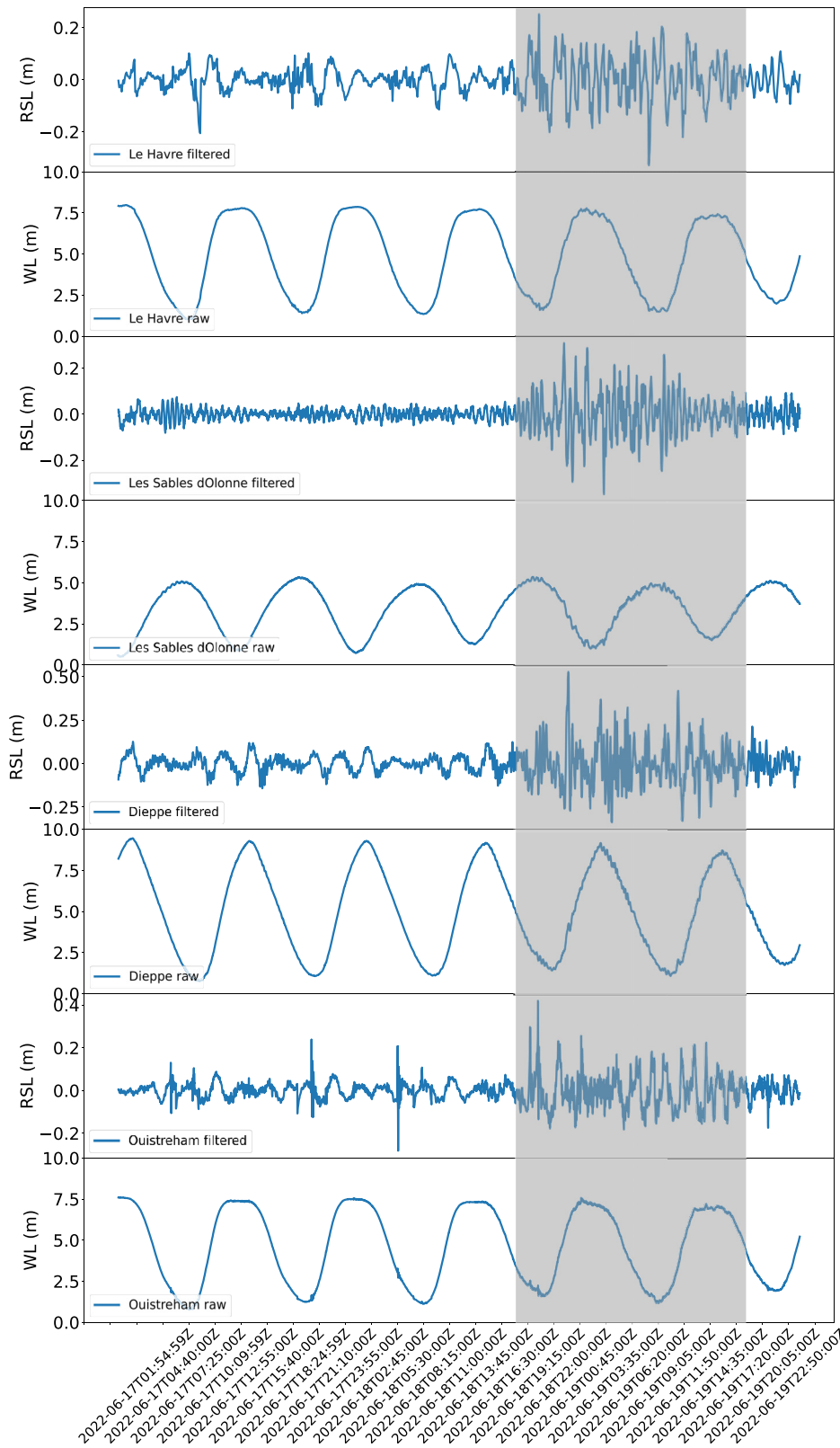
**FIG. 13.** De-tided and high-pass filtered (Butterworth) records of the event of 18 June 2022 at Le Havre, Les Sables-d'Olonne, Dieppe, and Ouistreham. Top plot of each panel shows the raw observed sea water level at the tide gauge. Data are recorded every minute, except for Le Havre, which was recorded every 5 min.
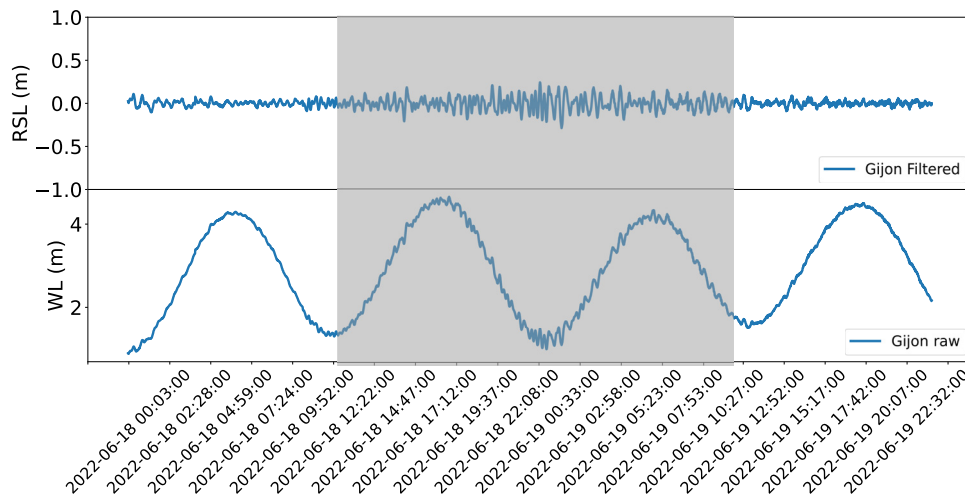
02 October 2023 13:25:23

**FIG. 14.** De-tided and high-pass filtered (Butterworth) records of the event of 18 June 2022 at Gijon. The bottom plot shows the raw observed sea water level at the tide gauge. Data are recorded every minute.

The signature of the sea level perturbation associated with the meteotsunami events can be observed at all locations between 18 and 19 June. The signal is particularly noticeable at Union Hall, where the main perturbation occurred at a frequency of around 1.35 cycles per hour (45 min), with some superharmonics occurring at around noon. Given the fact that this is a particularly elongated water inlet with approximately 5.5 km length and 0.5 km width, the high-frequency perturbations at those scales can be linked to the resonance properties of the water body. The opposite case can be observed at Wexford, where some subharmonic oscillations of around 0.5 cycle/hour were observed. This is likely due to the fact that the main body of water at Wexford is an open semi-quadratic inlet with a characteristic dimension of around 5 km, i.e., much wider than Union Hall. Similar conclusions can be drawn for the wavelet power spectrum at locations in the UK (Milford Haven), France (Brest, La Cotiniere, Le Crouesty), and Spain (Gijon), not reported here for the sake of brevity.

### C. Tidal change rates

We also investigated the tidal change rates for three of the Irish tidal stations, namely Ballycotton, Castletownbere, and Union Hall, for the dates ranging from 9 to 19 June inclusive. Over this period, the mean tidal change per 5 min for all stations was found to be a decrease of approximately $0.2 \times 10^{-3}$ m per 5 min. The mean and the mode for all stations was found to be 0.00 m per 5 min and the rate of change was normally distributed. By far the largest fluctuations can be seen in Fig. 18 on 18 June. The largest increases and decreases for each location are as follows:

- Ballycotton: increase of 0.35 m per 5 min, decrease of 0.34 m per 5 min.
- Castletownbere: increase of 0.35 m per 5 min, decrease of 0.32 m per 5 min.
- Union Hall: increase of 1.19 m per 5 min, decrease of 0.67 m per 5 min.

The rates of change at Union Hall were the most significant. The increase of 1.19 m per 5 min occurred at 2:45 pm on 18 June and the

decrease of 0.67 m per 5 min occurred just before at 2:40 pm on the same day, which correspond well to the eyewitness reports (see again Sec. II).

## V. NUMERICAL SIMULATION

Simulations of the 18 June 2022 meteotsunami along the south of Ireland were carried out using Volna-OP2 (Reguly *et al.*, 2018), which solves the non-linear shallow water equations (NSWE) using a finite volume discretization and has been validated against traditional tsunami benchmark tests, see Giles *et al.* (2020). The methodology as described by Kubota *et al.* (2021) was followed here, namely, the spatio-temporal sea surface pressure $p_s(x, y, t)$ acts as the source term. The seawater density is assumed to be $\rho_0 \approx 1020$ kg/m³; hence, a pressure change of 1 hPa is equal to a sea-height change of 1 cm. The GEBCO 2022 data are used for the bathymetry. A non-uniform triangular mesh for the region (resolution varies from 10 km to 500 m) is used, generated by the OceanMesh software (Roberts *et al.*, 2019).

### A. Surface pressure disturbance

The surface pressure field $p_s(x, y, t)$ was modeled as a sine pulse traveling from the south west to the east coast of Ireland. The shape and direction of travel of the pressure wave was motivated by the pressure disturbances observed at the various observation stations (Fig. 4). The direction of travel ($\theta = 43.3°$) found in Sec. III A 2 is used to carry out a rotation of the coordinate system $[(x, y) \mapsto (x', y')]$. The analytical expression for the sine pulse in the rotated frame is given as follows:

$$p_s(x', y', t) = P_0 \sin\left[k(x' - r)\right]\tau(t)$$

$$\times \begin{cases} 1 & \text{if } |x' - r| < \dfrac{L_0}{2} \text{ and } y_b \leq y' \leq y_t, \\ \gamma(y' - y_b) & \text{if } |x' - r| < \dfrac{L_0}{2} \text{ and } y' < y_b, \\ \gamma(y' - y_t) & \text{if } |x' - r| < \dfrac{L_0}{2} \text{ and } y' > y_t, \end{cases} \quad (3)$$
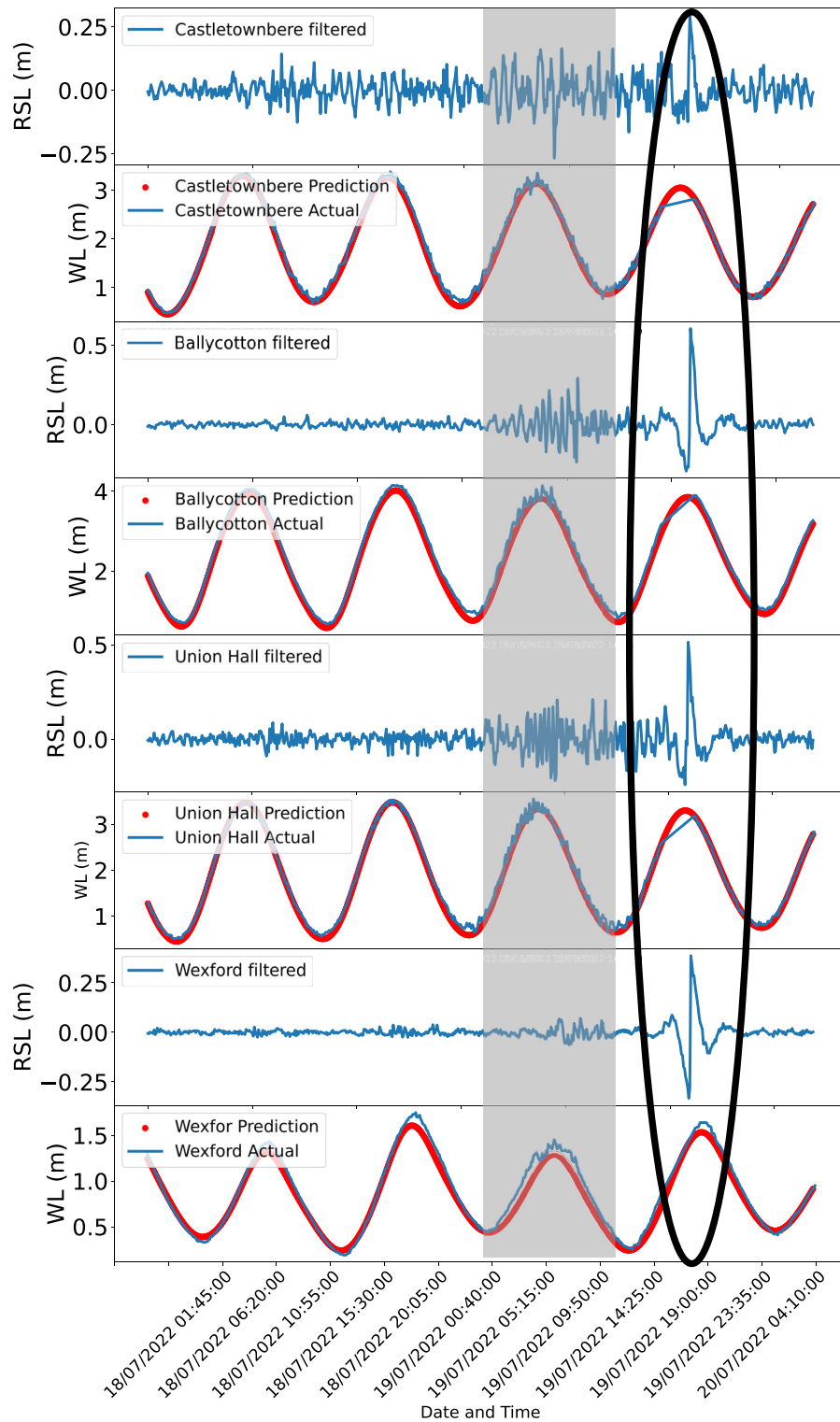
**FIG. 15.** De-tided and high-pass filtered (Butterworth) records of the event of 19 July 2022 at four tidal gauges around the south coast of Ireland. Data are recorded every 5 min. The gray shaded area highlights the time of the suspected second meteotsunami. The solid ellipse highlights the time period between ∼7:00 pm and ∼11:30 pm on 19 July, where all tide gauges are missing data. Therefore, results in the circled region are not reliable.
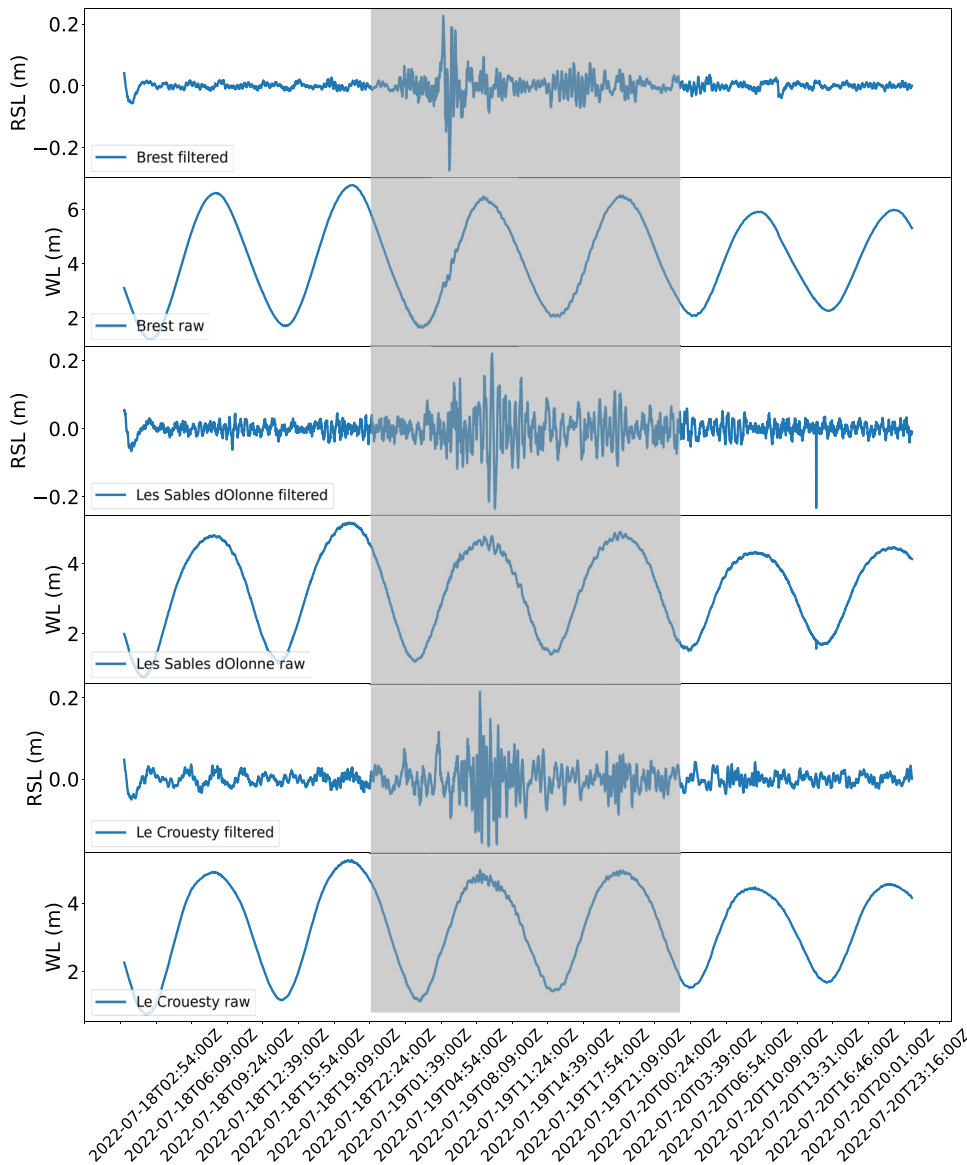
**FIG. 16.** De-tided and high-pass filtered (Butterworth) records of the event of 19 July 2022 at Brest, Les Sables-d'Olonne, and Le Crouesty. The bottom plot of each panel shows the raw observed sea water level at the tide gauge. Data are recorded every minute. The shaded region highlights the time of the event.

$$\tau(t) = 1 - \exp\left[-\left(\frac{t}{0.5T_0}\right)^2\right], \tag{4}$$

$$\gamma(y) = \exp\left[-\left(\frac{y}{\mu}\right)^2\right], \tag{5}$$

where $r(t) = R_0 + V_0 t$ defines the edge of the disturbance, and $k = \frac{2\pi}{L_0}$. The free parameter values of the optimal simulation run are as follows: $P_0 = -1.5$ hPa, $T_0 = 200$ s, $L_0 = 372$ km, $R_0 = 50$ km, $V_0 = 51.7$ m/s, $y_t = 200$ km, $y_b = -100$ km, and $\mu = 25$ km. Therefore, the length of the wave perpendicular to the direction of travel is set to 300 km, and an exponential tapering [Eq. (5)] is imposed at both ends to avoid an unrealistic discontinuity along this axis.

Figure 19 shows a comparison between the simulated air pressure perturbation and data recorded at the five weather stations in the south of Ireland. The data are filtered using a Butterworth high-pass filter. Note that the observed and simulated pressures for the five station locations exhibit good agreement.

## B. Resultant wave propagation

Figure 20 shows snapshots of the wave height across the domain. The initial wave (upper left subplot) mirrors the overall shape and extent of the prescribed atmospheric disturbance [Eqs. (3)–(5)]. The influence of the continental shelf and coastal bathymetry on the propagation of the generated wave is captured in the other subplots. The
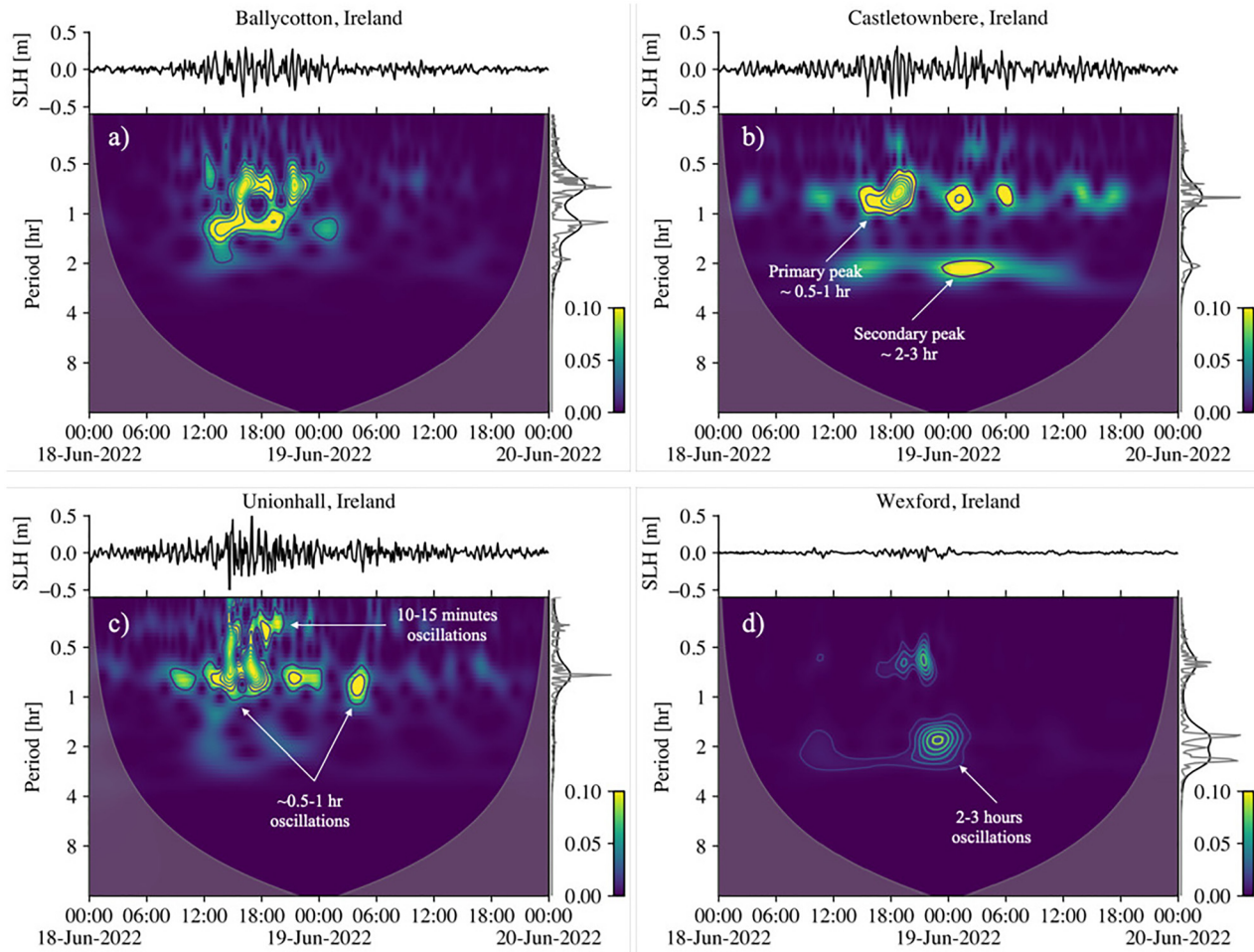
**FIG. 17.** Wavelet power spectrum corresponding to (a) Ballycotton Harbour, (b) Castletownbere Port, (c) Union Hall Harbour, and (d) Wexford Harbour. The color scale indicates the wavelet power spectral density in $m^2$/cph, where cph means cycles per hour. The shaded gray area is the cone of influence. The top insert of each panel shows the time series of the high-pass filtered sea level signal in metres. The right insert illustrates the time-integrated wavelet power (black line) and the Fourier power spectrum (gray line).

direction and length of a transect through the domain is also shown. The wave height along this transect is explored further in Sec. V C.

The tide gauge records, already discussed in Sec. IV, are compared with the results of the numerical simulations. We assume the start time to be the time the pressure wave arrived at Sherkin Island weather station (approximately 11.15 am on 18 June 2022). Figure 21 shows a comparison between the recorded and simulated data for the Irish coastline. Note that the arrival of the first wave at Union Hall and Castletownbere is captured well by the simulations, with Castletownbere showing a particularly good agreement. On the other hand, the wave amplitude is overestimated at Ballycotton, and the agreement at Wexford is poor. The Wexford tidal gauge is located within an enclosed tidal estuary, and with the bathymetry resolution used here, the location of the virtual gauge had to be placed closer to the mouth of the estuary so as to ensure that the gauge is located offshore. This is a significant simplification, which leads to the poor agreement for Wexford. For the other tidal gauges,

the aim is to capture the arrival of the first wave, as the faster oscillations that follow are likely due to harbor resonances. As the bathymetry resolution used here does not capture localized effects, we do not expect to simulate these resonant waves. Such a level of comparison would require high resolution bathymetry within the port and harbors, which is out of the scope of this preliminary modeling exercise.

We remark that the 18 June meteotsunamis in UK, Ireland, and France were likely generated by several localized pressure perturbations acting in different areas, originating within a larger low-pressure region over the North Atlantic Ocean. Due to these complex localized sources, a comparison of the simulation against the tidal gauges along the UK and France coastline is not carried out here. The sheer complexity of such a forcing system would require the implementation of a coupled atmosphere-ocean model. We remark that only very few coupled models have been tested with some success in the past: the WRF model coupled with ROMS in the BRIFS (Balearic RIssaga Forecasting
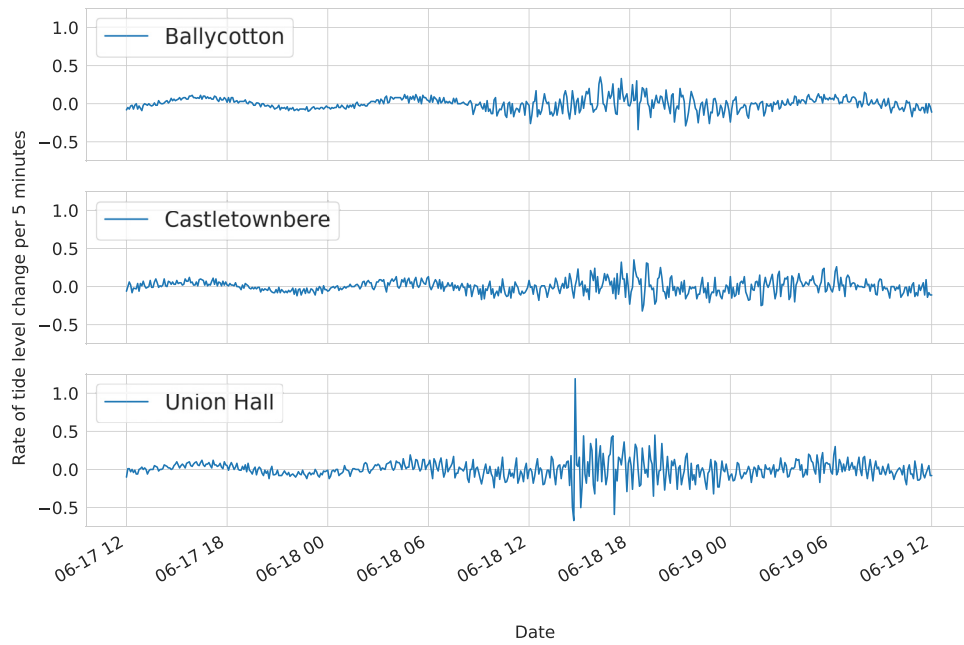
**FIG. 18.** Rate of tidal level change per 5 min on 17 and 18 June 2022 at several locations along the southern coast of Ireland. Level change is measured in metres.
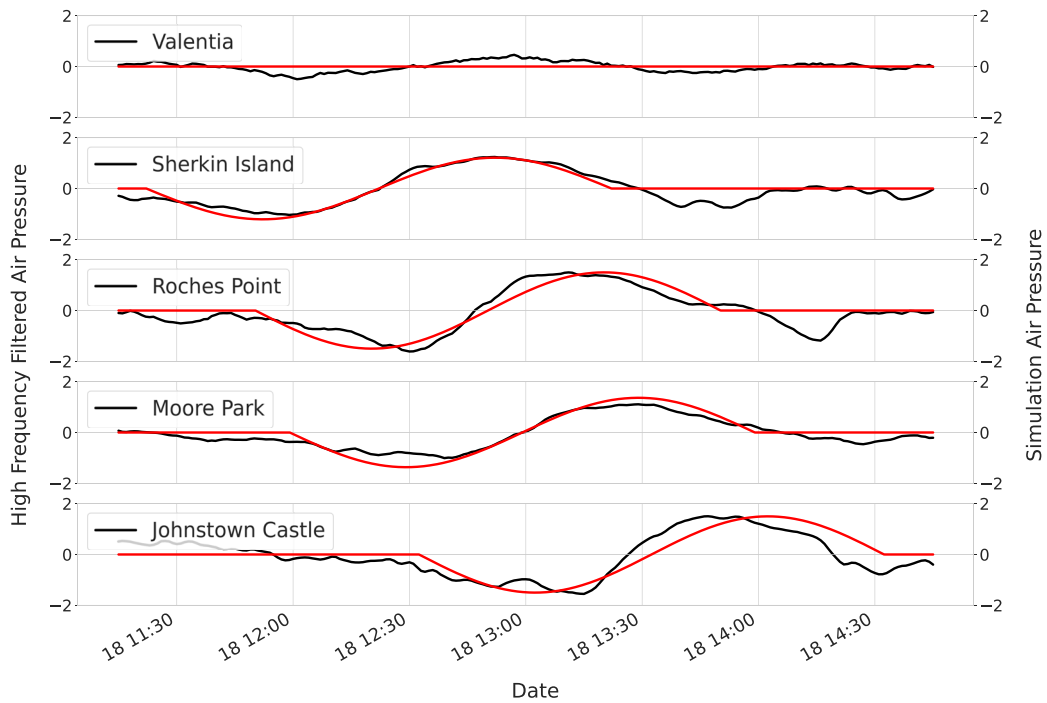
**FIG. 19.** Time series of the filtered air pressures at the respective weather stations (black) compared to simulated pressure at the virtual weather stations (red). Values are in hPa.
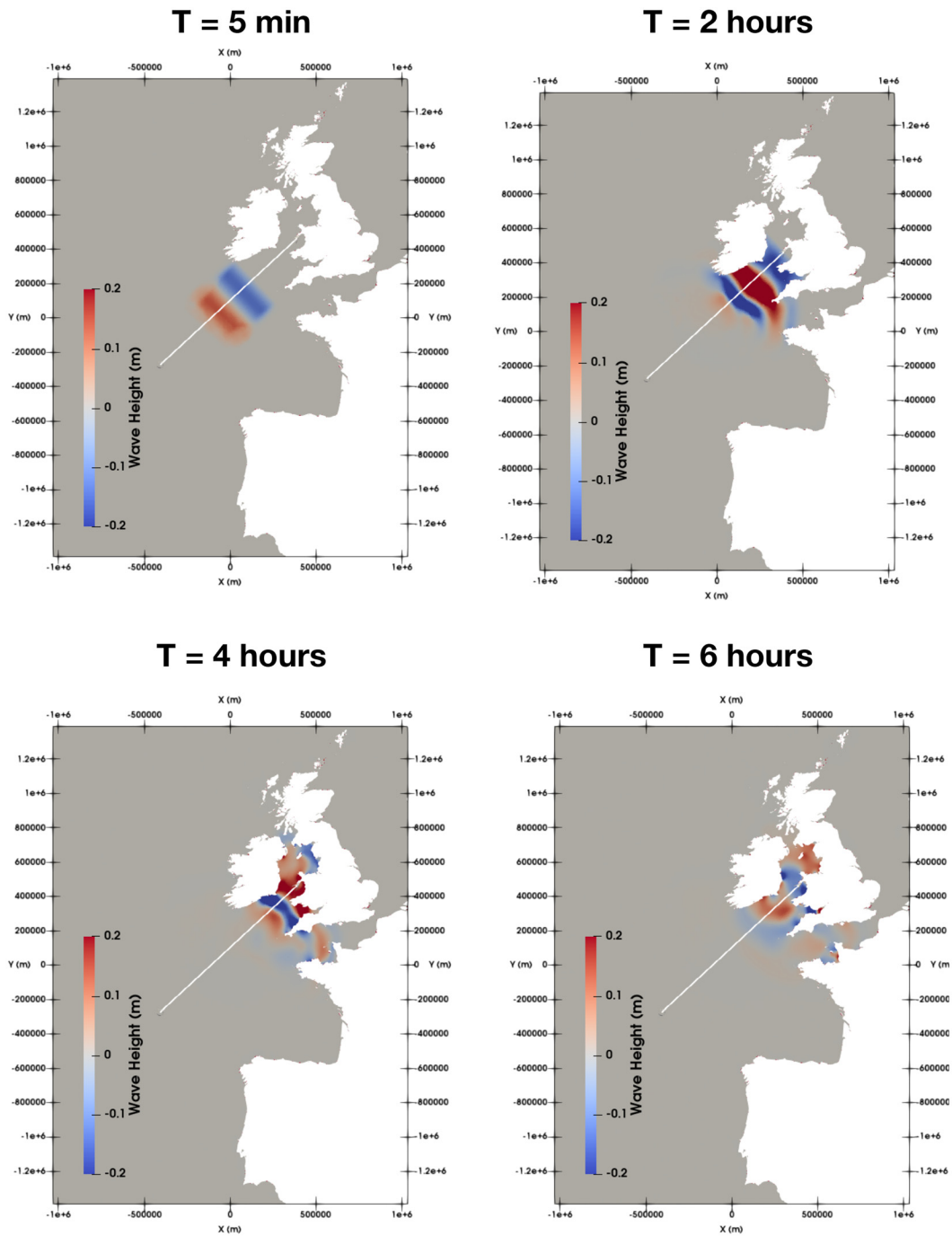
**FIG. 20.** Snapshots of the sea surface wave height at different time stamps across the domain. The direction and length of a transect through the domain is also shown. The wave heights along this transect are explored further in Sec. V C.

System) and WRF also coupled with ADCIRC in the Croatian meteotsunami early warning system (CMeEWS). The modeling suite is combined with an observational network of pressure sensors and tide gauges. However, BRIFS only provides simulations with atmospheric forcing at 4-km resolution, too coarse to represent meteotsunamis (Horvath et al., 2018). On the other hand, CMeEWS provides better performance but is computationally too expensive and was discontinued in 2019 (Tojčić et al., 2021).
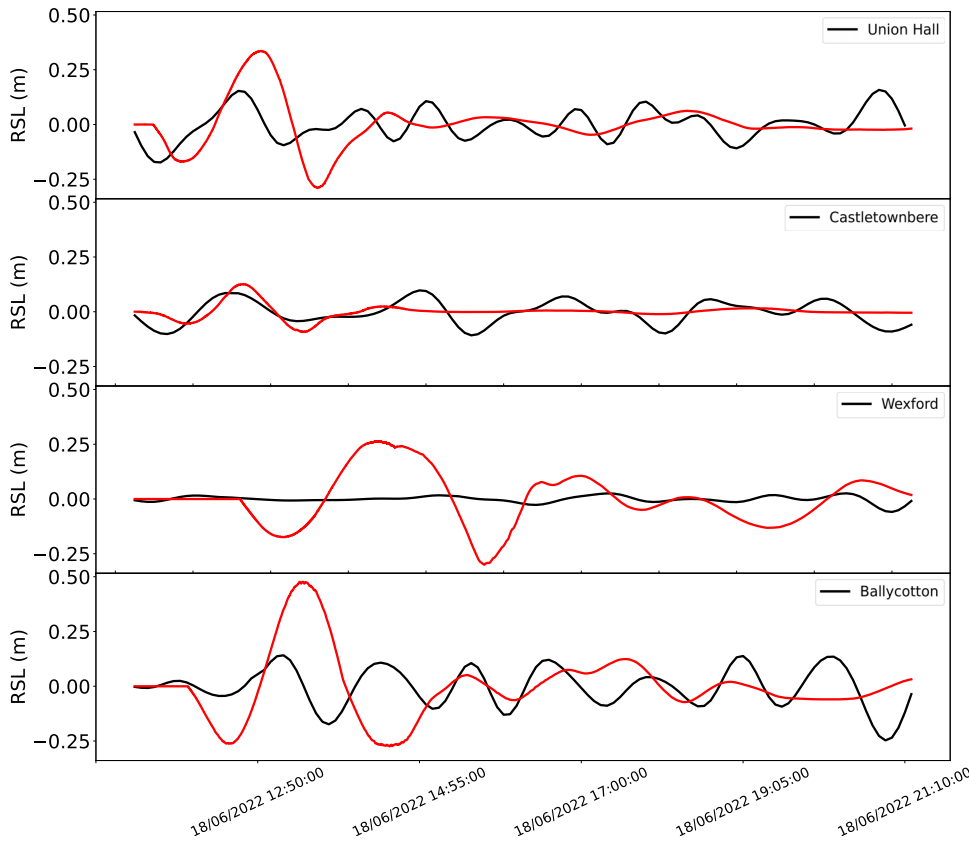
**FIG. 21.** Time series of the filtered coastal tide gauges in Ireland (black) compared to simulated wave heights at the virtual wave gauges (red).

## C. Influence of the atmospheric wave velocity

The influence of the atmospheric wave velocity on the amplification of the sea surface wave is investigated. The speed of the atmospheric wave is an important attribute of the Proudman resonance (Beisiegel and Behrens, 2022), which is suggested to be the dominant factor in the amplification of the wave along the southern Irish coastline for the event of 18 June 2022. Figure 22 shows the wave height along a transect of the domain through time with varying atmospheric wave speeds, again calculated with the numerical model of Sec. V B. The direction and length of the transect is represented in Fig. 20. Clearly, the speed of the atmospheric perturbation ($v$) plays an important role, and this relationship can be captured by the Froude number $Fr = v/\sqrt{gH}$, where $H$ is the depth, and $g$ is the acceleration due to gravity. Beisiegel and Behrens (2022) found that the maximum gain in amplitude occurs when $Fr = 1$. The bathymetry depth along the transect is not uniform, and it intersects with the continental (Celtic) shelf. However, the mean bathymetry value along the shelf section is 103 m. From Fig. 22, a speed of 31.7 m/s generates the largest amplification, which corresponds to an estimated Froude number of 0.997, when the mean value of the shelf bathymetry is used. The atmospheric perturbation speed of 51.7 m/s derived from the weather station data in Sec. III A and used for the numerical analysis in Sec. V B amplifies the initial disturbance but not to the same degree. Note that the wave crest amplification factor for 51.7 m/s is about 5, which is consistent with other meteotsunami

events, such as the 1979 Nagasaki bay (Japan) meteotsunami (Monserrat *et al.*, 2006).

Overall, our simulations represent a preliminary step to model the 18 June event. Improved models would need to consider several localized atmospheric pressure sources and a refined bathymetry model to be able to simulate higher frequency oscillations within inlets and harbors, which further amplify wave amplitude. The influence of various physical parameters on the amplification of the initial disturbance could also be further explored, such as the influence of the direction of travel of the atmospheric wave and its period.

## VI. DISCUSSION AND CONCLUSIONS

We investigated several occurrences of anomalous tidal activity in coastal waters of UK, Ireland, France, and Spain during Summer 2022. The first sighting of an anomalous tidal surge occurred on 18 June 2022 in Wales, followed by similar observations in Ireland, France, and Spain. Several anomalous long-wave events were also reported in UK in the morning of 19 July 2022, when tidal surges were observed in south England and Wales.

An analysis of surface and high-altitude air pressure fields reveals the presence of a low pressure region north of Ireland and the UK on 18 June, accompanied by a large area of precipitation. In addition, a strong jet-stream was observed over the south coast of Ireland, and through England and Wales. Such synoptic conditions are reminiscent of similar conditions recorded during historical meteotsunami events
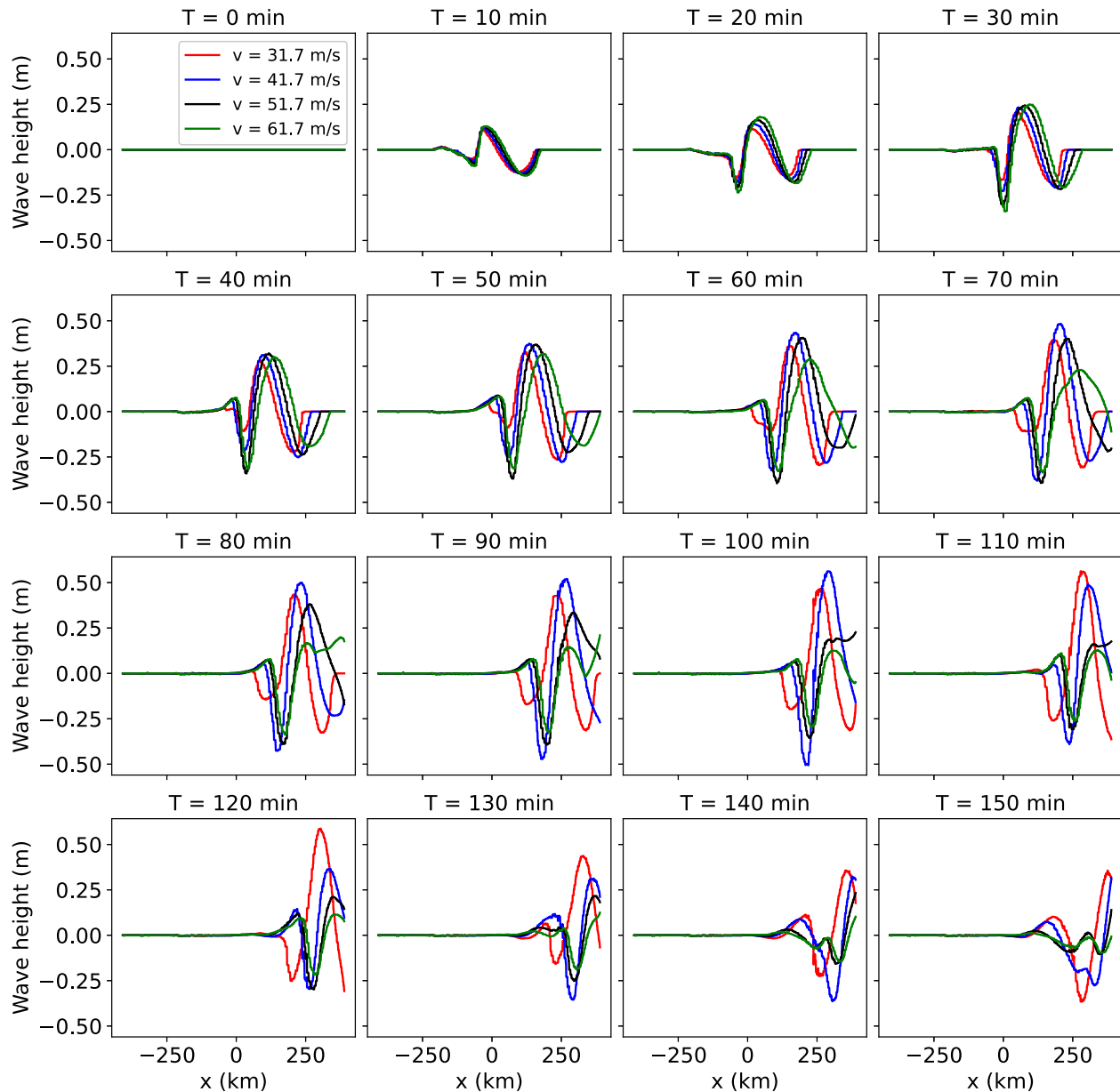
**FIG. 22.** Sea surface wave height along the transect through time for different atmospheric wave velocities.

in several regions of the world. An analysis of sea level oscillations in Ireland, UK, France, and Spain further confirms that the 18 June events were a series of meteotsunamis, propagating over several countries in Western Europe and triggered by localized pressure perturbations, originating within a low-pressure area on the North Atlantic Ocean. Local analysis for the south coast of Ireland suggests that Proudman resonance was the determinant mechanism that amplified the meteotsunami traveling eastward in the afternoon of 18 June.

A similar analysis for the 19 July events provides a less definite picture. There were no areas of low atmospheric pressure in the region,

and no high-altitude jet-stream was present. However, locally, strong winds were recorded in south Wales and the Bay of Biscay. An analysis of sea level oscillations suggests that the tidal surge events reported in the UK and the anomalous signals recorded in Ireland and France could be episodes of seiching triggered by infragravity waves, resonated subharmonically by wind waves.

It is interesting to note that Summer 2022 was the joint warmest ever recorded in UK, with mean temperature (17.1 °C) equaling that of 2018 (Met Office, 2022). Across Europe, the average temperature was the highest on record by a substantial margin of 0.4 °C over 2021

(Copernicus, 2022). Whereas a direct link between global warming and meteotsunamis has yet to be proven, it is known that storms feed off extra latent heat in the atmosphere, which has been shown to increase humidity, wind speed, and rainfall (NASA Earth Observatory, 2013). Such conditions are favorable to the genesis of meteotsunamis and infragravity waves. Therefore, in the context of increasing storminess and rising sea levels, it is important to consider how atmospheric-generated sea level oscillations can be better modeled and predicted.

Numerical simulations of the 18 June event were performed with Volna-OP2, which solves the non-linear shallow water equations using a finite volume discretization (Reguly et al., 2018; Giles et al., 2020). A synthetic pressure perturbation originating south of Ireland and matching pressure observations at local weather stations were used to force the model (Licer et al., 2017; Denamiel et al., 2018; Shi et al., 2020). The simulation results show good agreement with filtered coastal tide gauges in terms of maximum amplitude, though several inconsistencies remain. Most importantly, the non-dispersive nature of our solver, together with the mesh and bathymetry resolution used here, do not allow the reproduction of high-frequency oscillations in inlets and bays. An analysis on the influence of the atmospheric wave velocity on the amplification of the sea surface wave height is presented. These results showcase the importance of "tuned" parameters to enable the occurrence of resonance phenomenon.

Due to the sheer complexity of the atmospheric system generating the meteotsunamis on 18 June, and the equally challenging size and bathymetry of the region, the high spatio-temporal resolution needed to model the atmospheric process couples with the fine resolution required to model wave propagation. The intricacy of such a system would require sophisticated, coupled atmospheric-ocean solvers (Šepić et al., 2016). Since meteorological tsunamis are strongly amplified by small-scale topography features, such as bays and harbors, a reliable modeling tool requires a resolution higher than 20 m to capture resonant processes. These requirements result in extremely high computational costs. Such a challenge is so difficult that only a few coupled models have been developed for specific regions of the world (Balearic, Adriatic Sea), and virtually no coupled models at present can be applied globally. Our simulations provide a starting point and would need to be improved by considering several localized pressure sources and a more detailed bathymetry. This is the object of ongoing research.

Finally, we remark that some of the difficulties we encountered in providing a clear cut classification of the 19 July events are due to the lack of proper tide gauge measurements in UK. As already highlighted by Thompson et al. (2020), the UK records tidal gauge data at 15-min intervals, which is much higher than other European countries, e.g., Ireland (5 min) and France (1 min). The large sampling periods used in UK do not allow the recording of meteotsunamis, which have periods in the range of 10 min. In light of an increasing meteotsunami activity in the North Atlantic Ocean, possibly fuelled by global warming and climate change (Thompson et al., 2020; Williams et al., 2021b), it is strongly advised that the UK adopts real-time recording of tidal gauge data. More generally, we emphasize the need to have early warning systems including meteotsunami events along Irish, UK, and French coasts, knowing the difficulties encountered while trying to forecast such events in other regions with BRIFS in the Balearic Sea (Renault et al., 2011; Mourre et al., 2021) and AdriSC in the Adriatic Sea (Denamiel et al., 2019b; 2019a; Tojčić et al., 2021).

## AUTHOR DECLARATIONS
### Conflict of Interest

The authors have no conflicts to disclose.

### Author Contributions

**Emiliano Renzi:** Conceptualization; Investigation; Resources; Writing – original draft; Writing – review & editing. **Claire Bergin:** Data curation; Investigation; Methodology; Resources; Writing – original draft; Writing – review & editing. **Tatjana Kokina:** Data curation; Investigation; Methodology; Resources; Writing – original draft; Writing – review & editing. **Daniel Santiago Peláez-Zapata:** Data curation; Investigation; Methodology; Resources; Writing – original draft; Writing – review & editing. **Daniel Giles:** Data curation; Software; Writing – original draft; Writing – review & editing. **Frédéric Dias:** Conceptualization; Funding acquisition; Methodology; Writing – review & editing.

## DATA AVAILABILITY

The data that support the findings of this study are available within the article.

## REFERENCES

Ardhuin, F., Rawat, A., and Aucan, J., "A numerical model for free infragravity waves: Definition and validation at regional and global scales," Ocean Modell. **77**, 20–32 (2014).

Beisiegel, N. and Behrens, J., "Numerical testcases to study Proudman resonance using shallow water models," in ECCOMAS Congress 2022, 8th European Congress on Computational Methods in Applied Sciences and Engineering, 2022.

Bertin, X., de Bakker, A., van Dongeren, A. et al., "Infragravity waves: From driving mechanisms to impacts," Earth Sci. Rev. **177**, 774–799 (2018).

Copernicus, see https://climate.copernicus.eu/copernicus-summer-2022-europes-hottest-record for "Copernicus: Summer 2022 Europe's hottest on record" (last accessed November 24, 2022).

Cornwall Live, see https://www.cornwalllive.com/news/cornwall-news/incredible-tide-surge-porthleven-harbour-7360359 for "Rare phenomenon at Porthleven sends tsunami-like waves crashing into harbour" (last accessed August 22, 2022).

Daily Post, see https://www.dailypost.co.uk/news/north-wales-news/bizarre-water-surges-anglesey-beaches-24539730 for "'Bizarre' water surges on Anglesey beaches could have been rare 'meteotsunami'" (last accessed August 22, 2022).

Denamiel, C., Šepić, J., Huan, X., Bolzer, C., and Vilibić, I., "Stochastic surrogate model for meteotsunami early warning system in the Eastern Adriatic sea," J. Geophys. Res.: Oceans **124**, 8485–8499, https://doi.org/10.1029/2019JC015574 (2019a).

Denamiel, C., Šepić, J., Ivanković, D., and Vilibić, I., "The Adriatic Sea and Coast modelling suite: Evaluation of the meteotsunami forecast component," Ocean Model. **135**, 71–93 (2019b).

Denamiel, C., Šepić, J., Schultz, D., and Vilibić, I., "Impact of geomorphological changes to harbor resonance during meteotsunamis: The Vela Luka Bay test case," Pure Appl. Geophys. **175**, 3839–3859 (2018).

Dias, F., Dutykh, D., O'Brien, L., Renzi, E., and Stefanakis, T., "On the modelling of tsunami generation and tsunami inundation," Procedia IUTAM **10**, 338–355 (2014).

Giles, D., Kashdan, E., Salmanidou, D. M., Guillas, S., and Dias, F., "Performance analysis of Volna-OP2—Massively parallel code for tsunami modelling," Comput. Fluids **209**, 104649 (2020).

Heidarzadeh, M., Šepić, J., Rabinovich, A., Allahyar, M., Soltanpour, A., and Tavakoli, F., "Meteorological tsunami of 19 March 2017 in the Persian Gulf: Observations and analyses," Pure Appl. Geophys. **177**, 1231–1359 (2020).

Horvath, K., Šepić, J., and Prtenjak, M. T., "Atmospheric forcing conducive for the Adriatic 25 June 2014 meteotsunami event," Pure Appl. Geophys. **175**, 3817–3837 (2018).

Irish Times, https://www.irishtimes.com/ireland/2022/06/19/locals-perplexed-by-sight-of-tide-going-the-wrong-way-off-cork-coast/ for "Locals perplexed by sight of tide going the wrong way' off Cork coast" (last accessed August 22, 2022).

Kazeminezhad, M., Vilibić, I., Denamiel, C., Ghafarian, P., and Negah, S., "Weather radar and ancillary observations of the convective system causing the northern Persian Gulf meteotsunami on 19 March 2017," Nat. Hazards **106**, 1747–1769 (2021).

Kubota, T., Saito, T., Chikasada, N. Y., and Sandanbata, O., "Meteotsunami observed by the deep-ocean seafloor pressure gauge network off northeastern Japan," Geophys. Res. Lett. **48**, e2021GL094255, https://doi.org/10.1029/2021GL094255 (2021).

Levin, B. and Nosov, M., *Physics of Tsunamis*, 2nd ed. (Springer, Switzerland, 2016).

Licer, M., Mourre, B., Troupin, C., Krietemeyer, A., Jansá, A., and Tintoré, J., "Numerical study of Balearic meteotsunami generation and propagation under synthetic gravity wave forcing," Ocean Model. **111**, 38–45 (2017).

McCarthy, G. and Berry, A., "Observation of a meteotsunami on the south coast of Ireland," Weather **77**, 281–282 (2022).

Met Office, see https://www.metoffice.gov.uk/about-us/press-office/news/weather-and-climate/2022/joint-hottest-summer-on-record-for-england for "Joint hottest summer on record for England" (last accessed November 24, 2022).

Monserrat, S., Vilibić, I., and Rabinovich, A. B., "Meteotsunamis: atmospherically induced destructive ocean waves in the tsunami frequency band," Nat. Hazards Earth Syst. Sci. **6**, 1035–1051 (2006).

Mourre, B., Santana, A., Buils, A., Gautreau, L., Licer, M., Jansá, A., Casas, B., Amengual, B., and Tintoré, J., "On the potential of ensemble forecasting for the prediction of meteotsunamis in the Balearic Islands: Sensitivity to atmospheric model parameterizations," Nat. Hazards **106**, 1315–1336 (2021).

NASA Earth Observatory, see https://earthobservatory.nasa.gov/features/Climate-Storms/page2.php "Storms are getting stronger, 2013" (last accessed November 24, 2022).

NOAA, https://ngdc.noaa.gov/hazard/tsu_travel_time_events.shtml for "Tsunami travel time maps: Tsunami sources" (last accessed August 22, 2022).

O'Brien, L., Dudley, J. M., and Dias, F., "Extreme wave events in Ireland: 14 680 BP–2012," Nat. Hazards Earth Syst. Sci. **13**, 625–648 (2013).

O'Brien, L., Renzi, E., Dudley, J. M., Clancy, C., and Dias, F., "Catalogue of extreme wave events in Ireland: revised and updated for 14 680 BP to 2017," Nat. Hazards Earth Syst. Sci. **18**, 729–758 (2018).

Rabinovich, A. B., Šepić, J., and Thomson, R. E., "The meteorological tsunami of 1 November 2010 in the southern Strait of Georgia: A case study," Nat. Hazards **106**, 1503–1544 (2021).

Reguly, I. Z., Giles, D., Gopinathan, D., Quivy, L., Beck, J. H., Giles, M. B., Guillas, S., and Dias, F., "The VOLNA-OP2 tsunami code (version 1.5)," Geosci. Model Dev. **11**, 4621–4635 (2018).

Renault, L., Vizoso, G., Jansá, A., Wilkin, J., and Tintoré, J., "Toward the predictability of meteotsunamis in the Balearic sea using regional nested atmosphere and ocean models," Geophys. Res. Lett. **38**, L10601, https://doi.org/10.1029/2011GL047361 (2011).

Roberts, K. J., Pringle, W. J., and Westerink, J. J., "OceanMesh2D 1.0: MATLAB-based software for two-dimensional unstructured mesh generation in coastal ocean modeling," Geosci. Model Dev. **12**, 1847–1868 (2019).

Šepić, J., Vilibić, I., Alexander, R., and Monserrat, S., "Widespread tsunami-like waves of 23-27 June in the Mediterranean and Black Seas generated by high-altitude atmospheric forcing," Sci. Rep. **5**, 11682 (2015).

Šepić, J., Vilibić, I., and Monserrat, S., "Quantifying the probability of meteotsunami occurrence from synoptic atmospheric patterns," Geophys. Res. Lett. **43**, 10,377–10,384, https://doi.org/10.1002/2016GL070754 (2016).

Shi, L., Olabarrieta, M., Nolan, D., and Warner, J., "Tropical cyclone rainbands can trigger meteotsunamis," Nat. Commun. **11**, 678 (2020).

Sibley, A., "Meteotsunamis reported around Britain and Ireland, and northern France, 18–19 June 2022," Weather **77**, 279–280 (2022).

Tanaka, K., "Atmospheric pressure-wave bands around a cold front resulted in a meteotsunami in the East China Sea in February 2009," Nat. Hazards Earth Syst. Sci. **10**, 2599–2610 (2010).

Thomson, R. E. and Emery, W. J., *Data Analysis Methods in Physical Oceanography*, 3rd ed. (Elsevier Science, New York, 2014).

Thompson, J., Renzi, E., Sibley, A., and Tappin, D. R., "UK meteotsunamis: a revision and update on events and their frequency," Weather **75**, 281–287 (2020).

Tojčić, I., Denamiel, C., and Vilibić, I., "Performance of the Adriatic early warning system during the multi-meteotsunami event of 11–19 May 2020: An assessment using energy banners," Nat. Hazards Earth Syst. Sci. **21**, 2427–2446 (2021).

Torrence, C. and Compo, G. P., "A practical guide to wavelet analysis," Bull. Am. Meteorol. Soc. **79**, 61–78 (1998).

UNESCO, see http://www.ioc-sealevelmonitoring.org/ for "Sea Level Station Monitoring Facility" (last accessed September 8, 2022).

Williams, D., Horsburgh, K., Schultz, D., and Hughes, C., "Examination of generation mechanisms for an English Channel meteotsunami: Combining observations and modeling," J. Phys. Oceanogr. **18**, 103–120 (2019).

Williams, D., Horsburgh, K., Schultz, D., and Hughes, C., "Proudman resonance with tides, bathymetry and variable atmospheric forcings," Nat. Hazards **106**, 1169–1194 (2021a).

Williams, D. A., Schultz, D. M., Horsburgh, K. J., and Hughes, C. W., "An 8-year Meteotsunami Climatology across Northwest Europe: 2010–17," J. Phys. Oceanogr. **51**, 1145–1161 (2021b).